AA Technical Memorandum ERL WPL-47

THE USE OF RADAR OBSERVATIONS OF C_n^2 VS. HEIGHT TO DEDUCE HEIGHT PROFILES OF REFRACTIVE INDEX

E. E. Gossard

Wave Propagation Laboratory
Boulder, Colorado
December 1979

noaa NATIONAL OCEANIC AND ATMOSPHERIC ADMINISTRATION / Environmental Research Laboratories

NOAA Technical Memorandum ERL WPL-47

THE USE OF RADAR OBSERVATIONS OF C_n^2 VS. HEIGHT TO DEDUCE HEIGHT PROFILES OF REFRACTIVE INDEX

E. E. Gossard

Wave Propagation Laboratory
Boulder, Colorado
December 1979

UNITED STATES
DEPARTMENT OF COMMERCE

NATIONAL OCEANIC AND
ATMOSPHERIC ADMINISTRATION
Richard A. Frank, Administrator

Environmental Research
Laboratories
Wilmot N. Hess, Director

CONTENTS

THE USE OF RADAR OBSERVATIONS OF C_n^2 VS. HEIGHT TO DEDUCE HEIGHT PROFILES OF REFRACTIVE INDEX

E. E. Gossard

INTRODUCTION

The primary purpose of this memorandum is to examine the possibility of significantly improving the height resolution and accuracy of the standard radiometric retrieval methods by adding information from active radar sounding of the (clear) atmosphere.

The first step is to examine the energy and refractive index balance equations to determine whether useful relationships between C_n^2 (which can be measured by radar) and the refractive index profile (which is closely related to the temperature and humidity profiles of interest to the meteorologist) can be found that permit the (active) radar wind sounder to aid the (passive) radiometric retrieval of temperature and humidity profiles. For example, if it could be shown that C_ϕ^2 is proportional to $\partial\phi/\partial z$, $(\partial\phi/\partial z)^2$ or $(\partial\phi/\partial z)^3$, above the boundary layer (where ϕ is potential refractive index) the radar could be used to provide the profile of refractive index except for some constants that would have to be determined by radiometric retrieval — a far more tractable problem than trying to recover the whole profile radiometrically. The retrieval would then be carried out on the refractive index profile.

Most in-situ studies have been directed toward the optical refractive index, whose C_n^2 depends almost entirely on temperature. The measurement of radio refractive index requires either the use of an expensive, relatively bulky microwave refractometer or a fairly complicated combination of fast-response temperature and humidity sensors. If an aircraft is available, the microwave refractometer is the more practical device. Some actual radar data are available for studies of the radio refractive index structure. In this memorandum the optical refractive index data will be considered first; then radio refractive index in-situ measurements will be examined. Last, a case of radar observations will be analyzed. Some statistics of occurrence of radio

refractive index layer structure will then be presented and a tentative model will be proposed.

The purpose of this model is very different from models such as those of Hufnagel (1974) and of Van Zandt et al. (1978). We wish to use measured profiles of C_n^2 to aid in temperature-humidity profile retrieval. Whereas much of the effort in the models is directed toward some way of parameterizing the fine structure too small to be resolved by the radar, our goal is to measure the fine structure of the C_n^2 profile with a high resolution radar and use it to help retrieve the temperature and humidity gradients. Both the intensity and the morphology of the turbulent layering are of interest. In this paper we will present evidence that the intensity (C_n^2) is closely related to the height gradient of refractive index. However, the structure of the layer often suggests the presence of Kelvin-Helmholtz instabilities as seen in Figure 1-1. This type of morphology suggests shear across the layer, but is not the subject of this paper. However the orders of magnitude of variability in C_n^2 within the layer are to be noted.

A fairly fundamental relationship between structure parameter and gradient quantities is

$$C_\theta^2 = \alpha^2 \varepsilon^{-1/3} \varepsilon_\theta \, . \qquad (1\text{-}1)$$

This relationship is derived from dimensional reasoning like the ubiquitous 5/3 law, and it can therefore be expected to be fairly general. In (1-1) ε is the turbulent dissipation rate. Ottersten gives the value of 2.8 for α^2; θ can be considered to be any of a number of scalar quantities including potential temperature or potential refractive index. In general,

$$\varepsilon_\theta = - \overline{w'\theta'} \frac{\partial \theta}{\partial z} - \frac{1}{2} \frac{\partial}{\partial z} \overline{\theta'^2 w'} \qquad (1\text{-}2)$$

where w is vertical velocity, primes indicate perturbation quantities and overbars indicate an average.

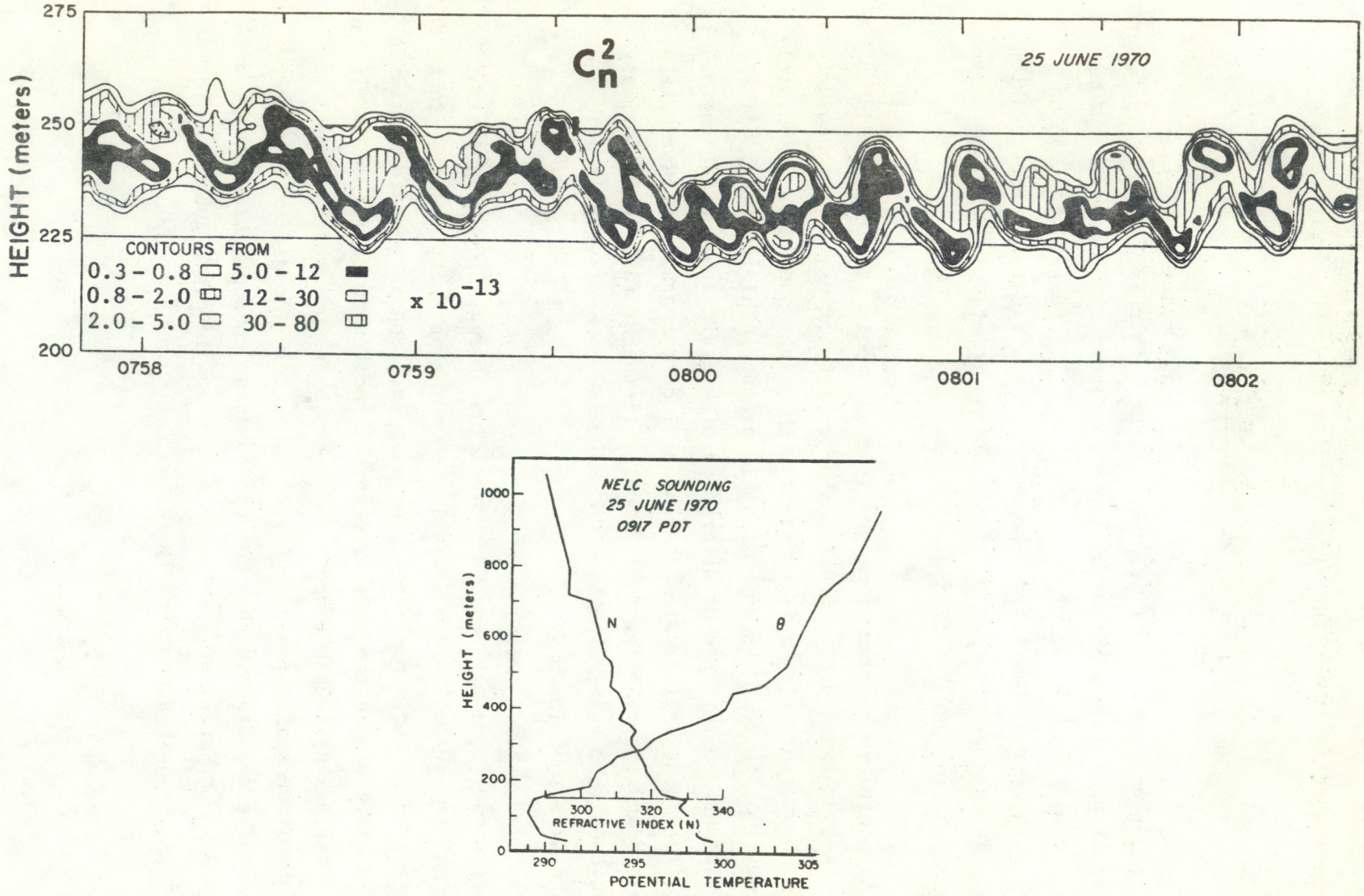

Figure 1-1. Fine structure of C_n^2 as measured by vertically pointing FM-CW radar (top frame) and corresponding radiosonde sounding data (bottom frame). Adapted from Metcalf (1975).

If the atmosphere is stable the first term on the right dominates and

$$C_\theta^2 = -\alpha^2 \varepsilon^{-1/3} \overline{w'\theta'} \frac{\partial \overline{\theta}}{\partial z} \quad . \tag{1-3}$$

An important fact to note at once is that ε is raised to a small power (-1/3), so it need not be measured with great accuracy. An order of magnitude error in ε causes only a factor of 2 error in C_θ^2. Besides, it can be estimated with fair accuracy from the width of the radar Doppler velocity spectrum. We will therefore concentrate on the relationship of C_θ^2 to the height gradient $\frac{\partial \overline{\theta}}{\partial z}$ and the flux quantities.

It is useful to consider some possible assumptions that may lead to useful relationships. Under conditions of constant flux, as in the surface layer, the heat flux, $\overline{w'\theta'}$, is constant with height and it is immediately clear from (1-3) that C_θ^2 is approximately proportional to $\partial\overline{\theta}/\partial z$. If the flux is not constant, convergence or divergence of heat in some height regions is implied. This usually indicates that spatial or temporal readjustments are taking place and the temperature is locally rising or falling. A primary task should be to investigate how widespread and generally applicable the constant flux assumption may be.

Other assumptions may lead to the conclusion that C_θ^2 is approximately proportional to $(\partial\overline{\theta}/\partial z)^2$ or to $(\partial\overline{\theta}/\partial z)^3$ depending on the properties that tend to be conserved in the atmosphere. For example, suppose a scale of mixing L is defined analogous to the mean free path in molecular diffusion. This is the classical mixing length concept which has been superseded by more rigorous treatments of diffusion physics. However, the different concepts lead to similar results and this concept contains considerable intuitive insight. Suppose a parcel of air is taken from one level to another. The situation is as shown schematically in the following sketch.

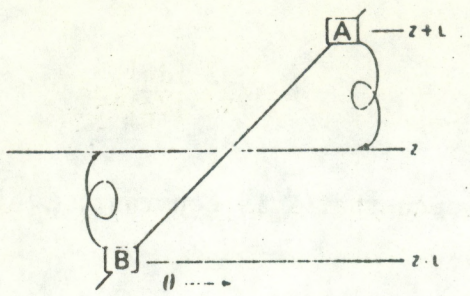

Let the sloping line segment represent a portion of the height profile of potential temperature. If an air parcel A with potential temperature θ_2 is mixed downward a distance L, it will cause a perturbation in θ at the new level of $L\, d\bar{\theta}/dz$. In like manner a parcel B of potential temperature θ, will cause a perturbation in θ, when mixed upward, of the same magnitude but of opposite sign. Similarly if a parcel A has a higher velocity than parcel B, the two parcels will converge if B is slightly behind A and diverge if B is ahead of A and the perturbation at the new level is $2u' = 2L\left|du/dz\right|$. However, equal transverse velocity perturbations are required by continuity considerations, so

$$w' = L\left|\frac{d\bar{u}}{dz}\right|.$$

However, upward velocity perturbations are associated with lower temperatures, if $\partial\theta/\partial z > 0$; therefore

$$\overline{w'\theta'} = - L^2\left|\frac{du}{dz}\right| \frac{\partial\theta}{\partial z}$$

and Eq. (1-1) becomes

$$C_\theta^{\,2} = + \alpha^2\, \varepsilon^{-1/3}\, L^2 \left|\frac{du}{dz}\right| \left(\frac{\partial\theta}{\partial z}\right)^2 . \qquad (1\text{-}4)$$

It is reasonable to presume that du/dz and $d\theta/dz$ have approximately the same functional form in elevated layers, say $\mathrm{sech}^2(z/h)$, i.e., an Epstein layer. Therefore, if the mixing scale L is assumed to be constant, $C_\theta^{\,2}$ will be proportional to $(\partial\theta/\partial z)^3$.

On the other hand an "eddy coefficient" K is often defined such that

$$K = L^2 \left|\frac{du}{dz}\right|. \qquad (1\text{-}5)$$

If the mixing process is such that K is constant, C_θ^2 will be proportional to $(\partial\theta/\partial z)^2$.

In order to get insight into the mixing process occurring in elevated layers, the profile data were compared with the C_θ^2 data in those cases for which complete documentation was available to determine whether the 1st, 2nd, or 3rd power dependence of C_θ^2 vs. $\partial\theta/\partial z$ was most representative, or whether any of them applied.

ANALYSIS OF OPTICAL REFRACTIVE INDEX DATA SETS

Case of 5 October 1976 - Fairall et al. Data Set

The sounding data for this case were reported by Fairall et al. (1977) and are shown in Fig. 2-1. The gradient of potential temperature and the C_θ^2 data through the layer are given vs. height in the first three columns of Table 1. In Table 2-1 the two profiles of C_θ^2 have been algebraically averaged. Also, the slight ripple in temperature at 260 m height has been smoothed out, and the $d\theta/dz$ profiles have been shifted down in height by 10 m to match the maximum values of C_θ^2. We consider this height correction reasonable, because the profile data were acquired by balloon and the C_θ^2 data by aircraft, so agreement in height within 10 m would be exceptional.

Assuming C_θ^2 to be proportional to the 1st power of $\partial\theta/\partial z$, the flux $\overline{w'\theta'}$ was calculated for 10 m increments within the layer. The flux values are shown plotted in column three of Table 2-1. No obvious trend is evident - perhaps a slight bulge exists near the middle of the layer.

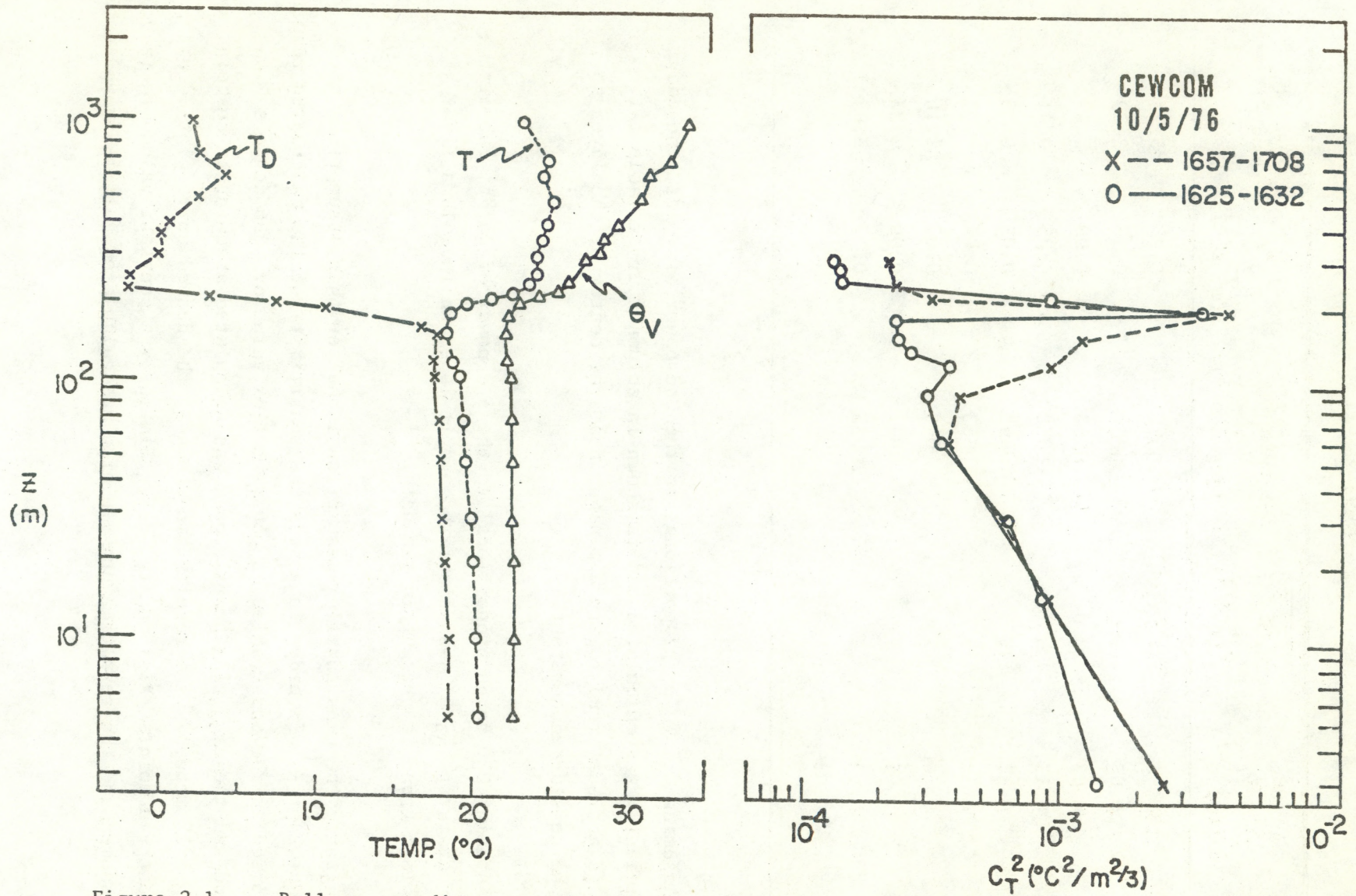

Figure 2-1. Balloon soundings of dewpoint (T_D), temperature (T) and virtual potential temperature θ_V measured by balloon (left frame) compared with aircraft sounding of C_T^2. Circled points are ascent; X's are descent. From Fairall et al. 1977, as plotted by S.D. Burk, private communication.

TABLE 2-1

Ht(m)	$\frac{d\theta}{dz}$ (deg m^{-1})	$\overline{C_\theta^2}$ ($m^{-2/3}$)	Flux (deg m s^{-1})	K (m^2 s^{-1})	$\frac{\Delta u}{\Delta\theta} L^2$
160	0.03	7.5×10^{-4}	-.0075	0.9	5.74
170	0.05	9.0	-.0062	0.13	2.29
180	0.07	12.0	-.0053	0.09	0.84
190	0.13	25	-.0068	0.053	0.41
200	0.17	45	-.0093	0.055	0.33
210	0.12	18	-.0053	0.045	0.37
220	0.06	7	-.0042	0.07	1.16
230	0.04	4	-.0037	0.09	2.23
240	0.03	2	-.0035	0.12	3.97
250	0.02				

Assuming C_θ^2 to be proportional to the 2nd power of $\partial\theta/\partial z$, the eddy coefficient K was calculated and is shown in column four of Table 2-1. There is a clear trend toward a minimum near the center of the layer so it can't be considered constant.

Assuming C_θ^2 to be proportional to the 3rd power of $\partial\theta/\partial z$, the mixing scale parameter $\frac{\Delta u}{\Delta\theta} L^2$ was calculated and it is shown in column five. A very clear trend is present in the data.

Clearly the constant flux assumption is better than assumptions of constant L or K. In order to assess the sensitivity of the calculated results to "noise" in the observables, a constant flux value of .006 deg m s^{-1} was assumed and the resulting profile of θ was calculated assuming an Epstein layer with h = 12 meters. The results are shown as the dashed curve plotted with the observed points (X's) in Fig. 2-2. Similarly a constant value of K = 0.067 was assumed and the resulting profile of θ was calculated. It is shown as the

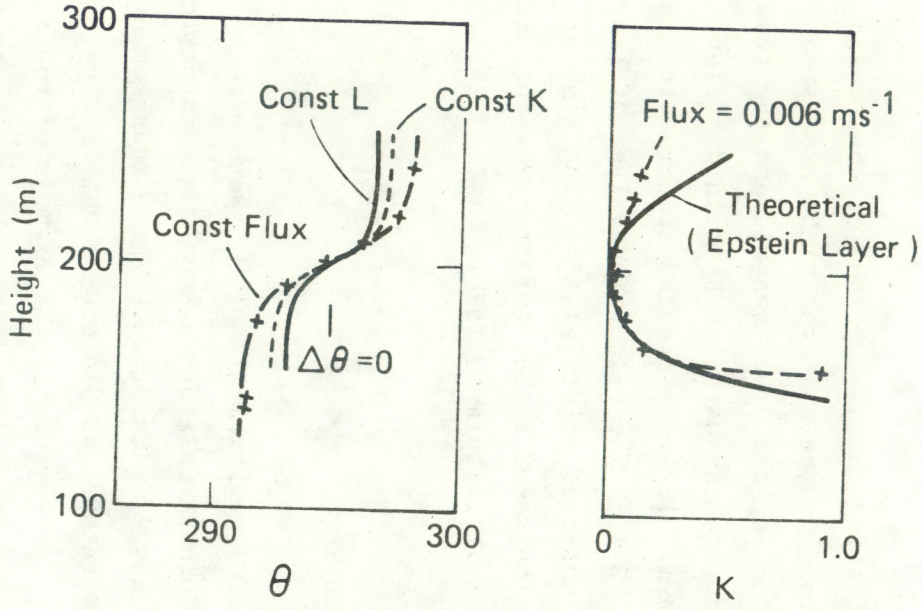

Figure 2-2. Left frame: Observed distribution of potential temperature vs. height (X's) compared with the constant flux assmumption (dash curve), constant K (short dashed curve) and constant L (solid curve). Right frame: Variation of K through layer assuming constant flux, theoretical (solid curve) and observed (dashed curve).

dotted curve in Fig. 2-2. Not only does the assumption of constant flux produce a better estimate of the observed profile than the constant K assumption, but it appears to lie within the range of natural variability in the real profile. Finally, a constant value of $(\Delta u/\Delta\theta)L^2 = 0.5$ was assumed and the calculated profile is shown as the solid curve. It should be noted that a value of $(\Delta u/\Delta\theta)L^2 = 0.11$ would have produced the $\Delta\theta$ of the observed profile, but this value is much lower than any of the observed values shown in Table 2-1.

Another way of testing the assumptions of constant flux or constant K against the observations is shown at the right hand side of Fig. 2-2. Here, a constant flux of .006 deg m s^{-1} was assumed and the resulting value of K vs. height was calculated assuming an Epstein distribution for $d\theta/dz$ imbedded in an isothermal layer. (See the temperature distribution above the inversion in Fig. 2-1.) The calculated values of K are shown as the solid curve, and the observed points as X's. The similarity in trend is clear, and the deviation seems to be comfortably within experimental scatter based on the inhomogeneity displayed in Fig. 1-1.

The Ochs-Lawrence Data Set

An extensive set of measurements of C_T^2 were made by Ochs and Lawrence (1972) through the southern California subsidence inversion and through a capping inversion at Haswell, Colorado. These measurements are especially valuable because temperature soundings were obtained by the aircraft simultaneously with the C_T^2 measurements. An example of their soundings is shown in Fig. 2-3, and their data on layer intensity ΔT, layer thickness h, maximum gradient $d\theta/dz$ and C_θ^2 are shown in Table 2-2. The thickness h is obtained from the width of the C_T^2 spike. It is the width at 0.41 of the peak value in accord with the Epstein profile. The maximum gradient $d\theta/dz$ was scaled graphically and is shown plotted vs. C_θ^2 in the left frame of Fig. 2-4. The corresponding plot of $\Delta T/h$ vs. C_θ^2 is shown in the right-hand frame. The difference in the plots indicates considerable subjectivity in choices of gradient in real atmospheric profiles. However, the clear tendency

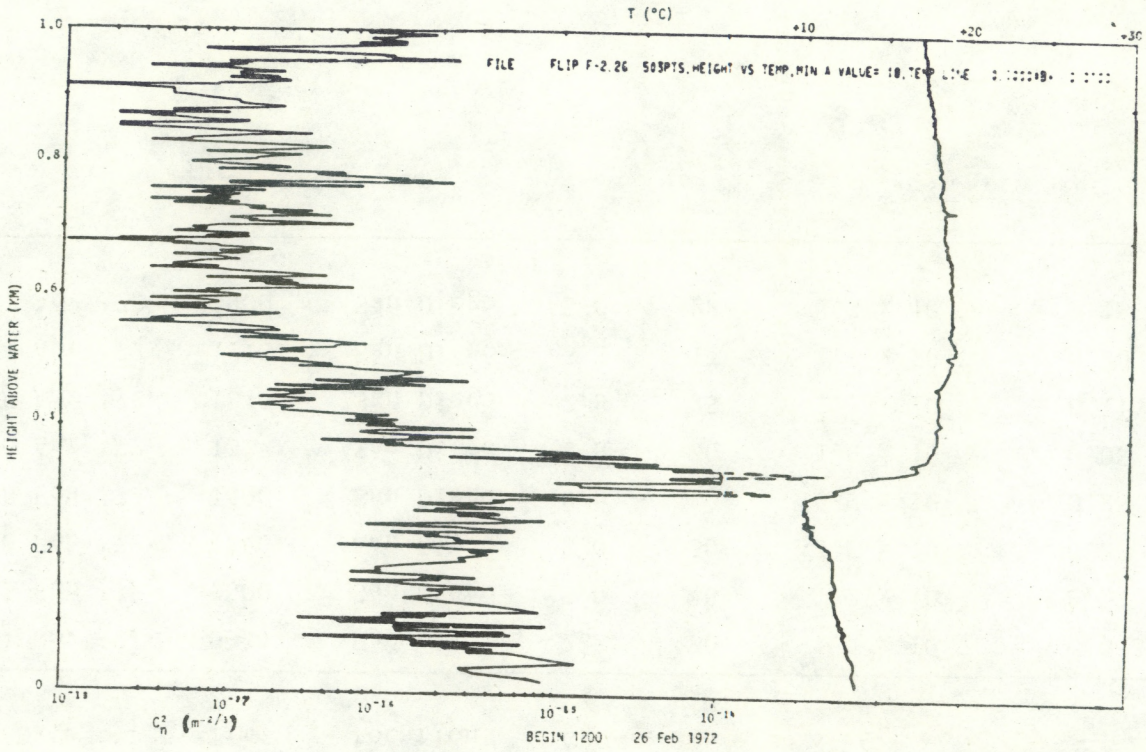

Figure 2-3. Height distribution of optical C_n^2 compared with temperature profile from aircraft measurements reported by Ochs and Lawrence, 1972. Instrumental cut-off at $C_n^2 = 10^{-14}$. Extrapolations shown by dashed curve at peak of cut-off.

TABLE 2-2

Layers Sounded by Ochs and Lawrence (1972)

Sounding No.	Date	Time	Location	ΔT	h (m)	C_θ^2	$\frac{\Delta T}{h}$	$\frac{d\theta}{dz}_{max}$
1	11 Nov '71	0934	Haswell	2.2	30	1.2×10^{-2}	0.073	.063
2	25 Feb '72	1500	San Diego	5.0	40	1.2×10^{-2}	0.125	0.11
3	26 Feb '72	1200	San Diego	8.0	30	3.5×10^{-2}	0.27	0.34
4	28 Feb '72	1400	San Diego	10.0	40	6.9×10^{-2}	0.25	1.0
5	20 Apr '72	1327	San Diego	1.5	30	1.0×10^{-2}	0.05	0.14
6	20 Apr '72	1840	San Diego	2.8	25	2.3×10^{-2}	0.11	0.11
7	21 Apr '72	1213	San Diego	3.5	17	1.7×10^{-2}	0.20	0.07
8	21 Apr '72	1900	San Diego	5.0	28	2.3×10^{-2}	0.18	0.31

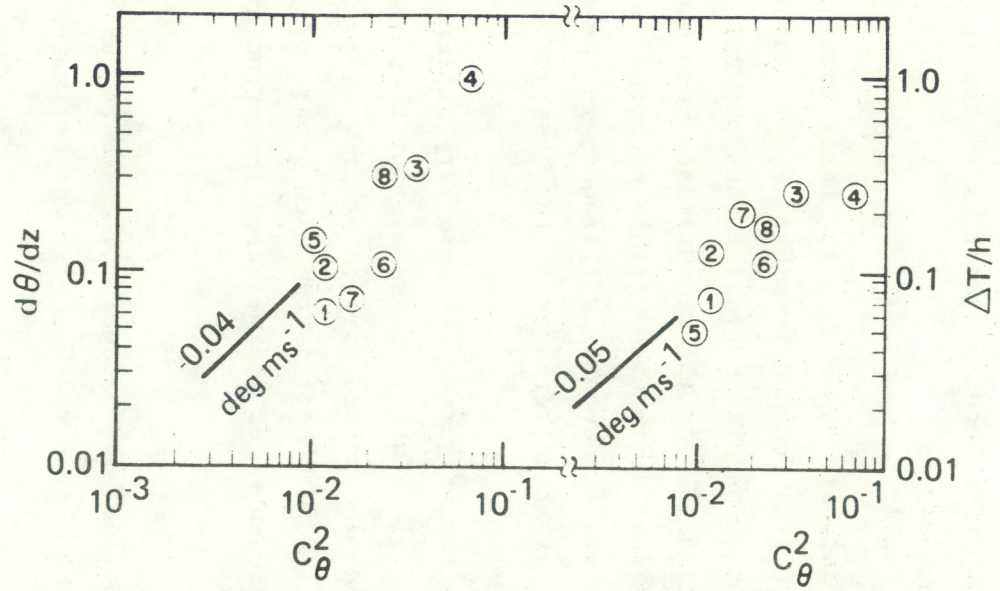

Figure 2-4. Measured values of maximum potential temperature gradient vs. temperature structure constant through inversion layers from data obtained by Ochs and Lawrence using aircraft-borne sensors. Both $d\theta/dz$ and $\Delta T/h$ are plotted for comparison because of the difficulty of scaling accurate values of gradient. The solid lines are labeled with the temperature flux implied by the data.

toward a slope of unity (rather than 2 or 3) again suggests that C_T^2 is proportional to the 1st power of the gradient rather than the 2nd or 3rd power. The Ochs and Lawrence data thus support the suggestion that the constant flux assumption may often be valid through these kinds of layers. Furthermore, the relatively small scatter of points on different days and times suggests that the fair weather downward heat flux may be a fairly conservative quantity, at least in some geographical areas; there is little evidence of a consistent difference in heat flux in the April data from that in the February or November data.

The Ochs-Lawrence data are remarkable for their internal consistency. However, the temperature flux deduced from Fig. 2-4 is about -0.04 m s^{-1}deg which is almost an order of magnitude greater than the value of about -0.006 found from the PG School data. As the measurements were made in approximately the same environment, a real difference of this magnitude would not be anticipated. There are several fundamental differences in the observation systems that may account for apparent differences in the observed data:

a) The techniques for measuring C_θ^2 were very different. The Ochs-Lawrence sensor was a single, fast-response element that measured temporal fluctuations. They were band-passed for scales of 7 cm to 70 m for the speed of the aircraft used. The PG School system used a pair of 2.5 micron platinum wires separated by about one meter and measured the structure function directly for a meter separation.

b) The noise level in the PG School measurements was about 4×10^{-4} and the correction in the measurements of C_θ^2 was estimated "after-the-fact."

c) A 5 second time constant was used in the RMS processing module for the PG School data prior to recording on a strip chart recorder thus introducing an algebraic averaging of data that is approximately log normally distributed.

Heat Flux from C_θ^2 Measurements

The flux of heat F_H in gram calories per square centimeter per second is

$$F_H = \rho C_p \overline{w'\theta'}$$

where the air density $\rho \simeq 0.24$ cal deg^{-1} gr cm^{-3} and the specific heat at constant pressure $C_p \simeq 0.24$ cal deg^{-1}. Therefore, from the Ochs-Lawrence data ($\overline{w'\theta'} \simeq 4$ deg cm s^{-1})

$$F_H = 1.18 \times 10^{-3} \text{ gr cal cm}^{-2} \text{ s}^{-1}$$

and from the Fairall et al. data ($\overline{w'\theta'} \simeq 0.6$ deg cm s^{-1})

$$F_H = 1.8 \times 10^{-4} \text{ gr cal cm}^{-2} \text{ s}^{-1}.$$

For an order-of-magnitude check, this value may be compared with Brunt's estimate of the outgoing flux of long wave radiation on a clear night in England as 2.1×10^{-3} gr cal cm^{-2} s^{-1}; roughly half of this would come from the soil and half would be contributed by the atmosphere through downward diffusive flux from air to the radiating soil interface. As another comparison, note that 1 gr cal = 4.185×10^7 ergs, so 10^{-3} gr cal cm^{-2} s^{-1} = 4.185×10^4 ergs cm^{-2} s^{-1}. Brunt estimates that on the average mechanical turbulence in the atmosphere dissipates 10^3 ergs cm^{-2} s^{-1}. It appears that the magnitudes of heat flux suggested by the C_θ^2 techniques are reasonable.

3. ANALYSIS OF RADIO REFRACTIVE INDEX DATA SETS

Case Study of 17 November 1976 - Thompson et al. Data Set

In measurements reported by Thompson et al. (1976) profiles up to 29,000 ft MSL were obtained in Florida and near Boulder Colorado using a microwave refractometer in an aircraft. Most of the soundings contained at least one strong gradient within the height range. An impressive exception to the usual layered profile occurred on 17 November 1976 during a slant

descent from 28,000 ft at Boulder, Colorado. On this day the temperature and refractive index profiles suggest a remarkably homogeneous atmosphere on this day as shown in Figures 3-1 and 3-2 taken from the Thompson et al., report. Because of its remarkable homogeneity, this case provided an opportunity to study the height distribution of refractive index quantities in the rare case of an ideally homogeneous atmosphere. We therefore examined it in some detail as a case study. The height distribution of C_n^2 is shown in Figure 3-3. If C_n^2 is plotted on log log paper the resulting plot relative to sea level is shown in Figure 3-4. The plot of N vs. height is shown as the dashed curve plotted on a log scale in Figure 3-5. The indicated straight line fit to the C_n^2 data gives

$$C_n^2 = 1.5 \times 10^{-13} z^{-4.13} \qquad \text{(MSL)} \qquad (3\text{-}1)$$

and the fit to the N(z) data gives

$$N = 301\ e^{-0.12z} \qquad \text{if z is km MSL} \qquad (3\text{-}2a)$$

or

$$N = 247\ e^{-0.12z} \qquad \text{if z is km AGL} \qquad (3\text{-}2b)$$

at Boulder. The temperature profile is well represented by

$$T = 308.4 - 8.74 \times 10^{-3} z.$$

For purposes of relating the refractive index to atmospheric dynamics the most useful refractive index quantity is the potential refractive index ϕ which is analogous to the potential temperature and potential vapor pressure. It is the refractive index of a parcel of air of fixed mass if brought adiabatically and without change in absolute humidity to the 1000 millibar pressure level. Thus it is conserved during motions that are adiabatic. It is a useful quantity to deal with for many purposes because short term atmospheric motions take place essentially adiabatically and without change in absolute humidity (unless near saturation).

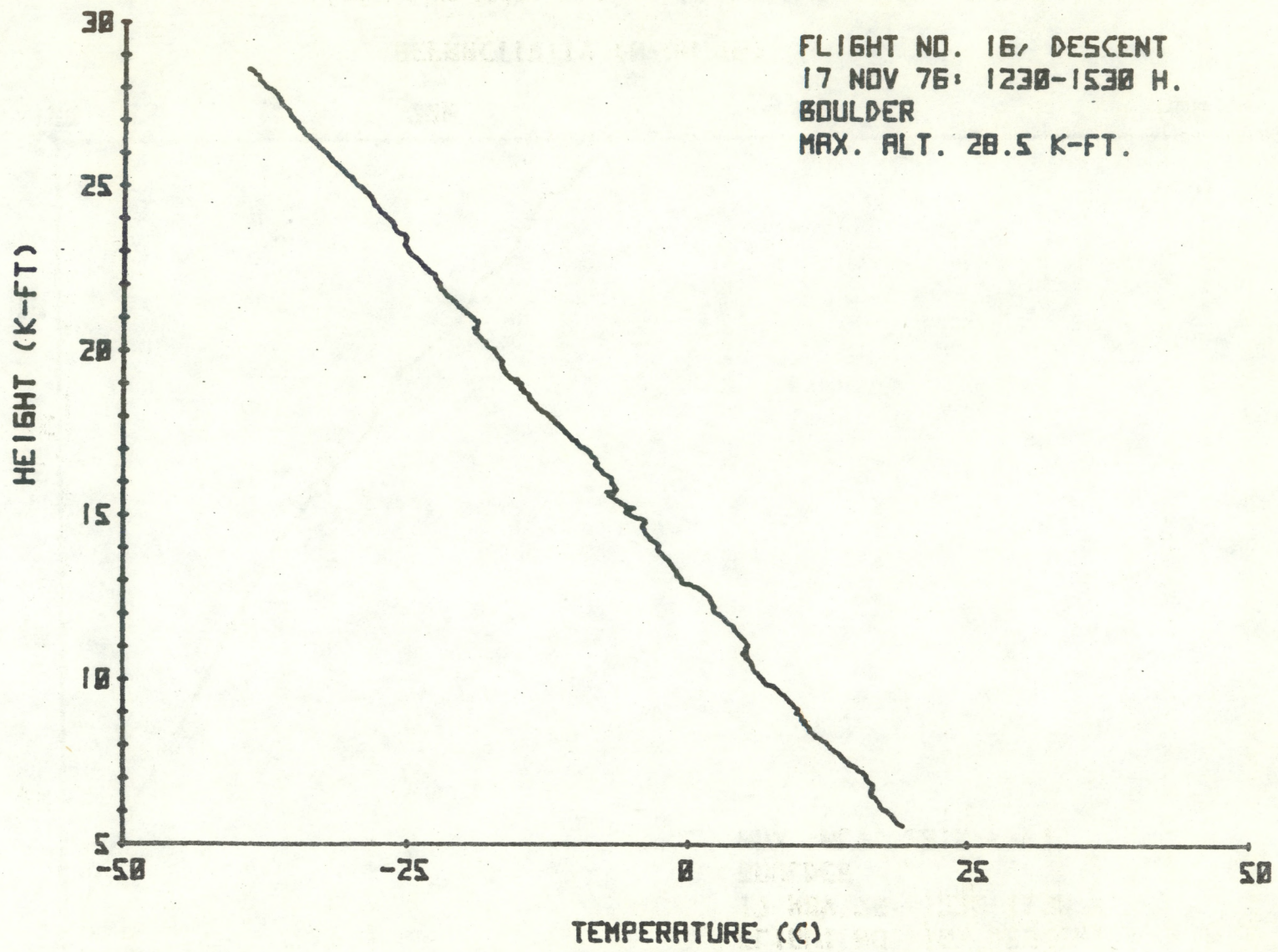

Figure 3-1. Temperature sounding reported by Thompson et al.

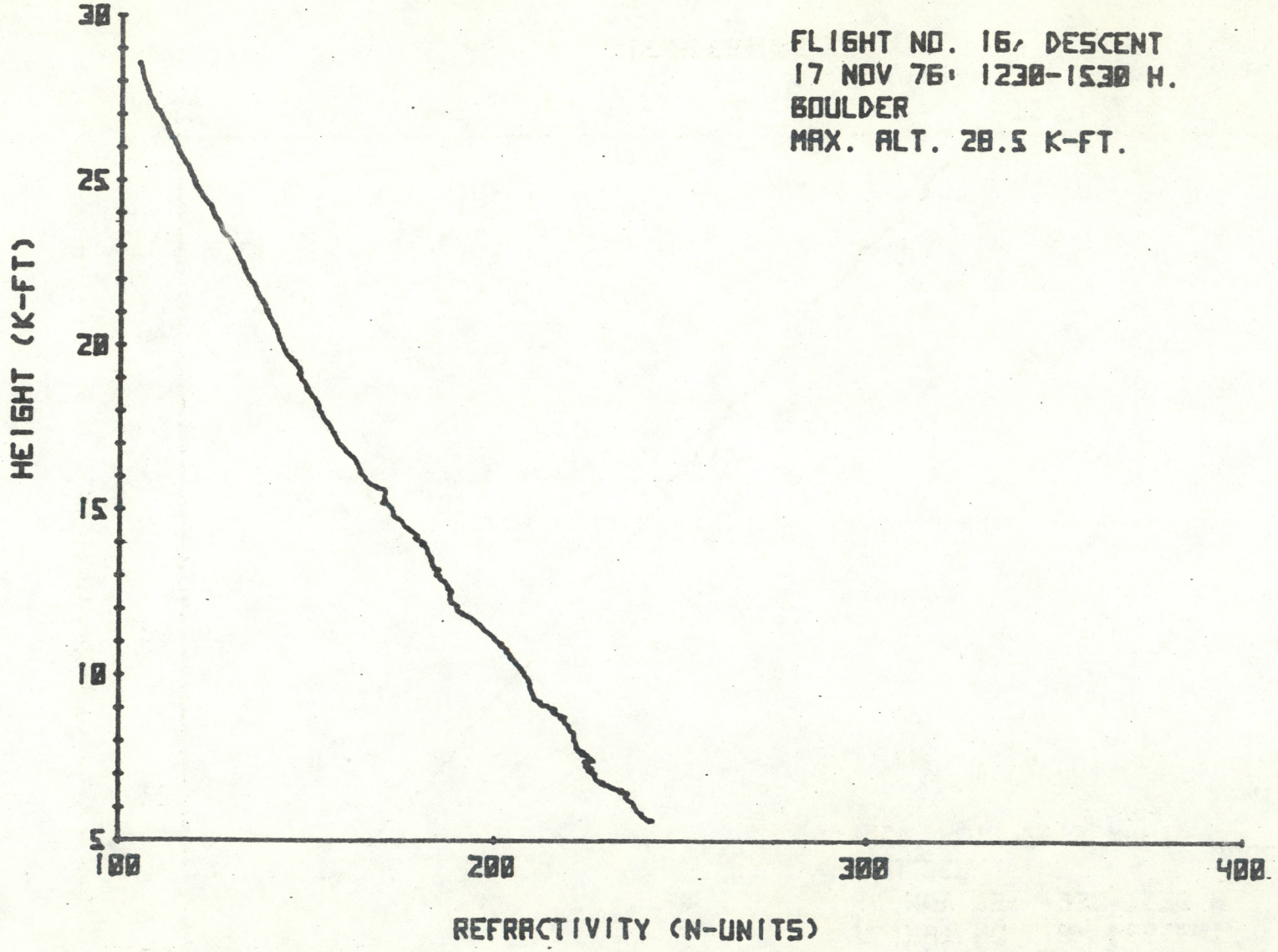

Figure 3-2. Refractive index sounding corresponding to temperature sounding of Figure 3-1. $N = (n-1) \times 10^{-6}$ where n is refractive index.

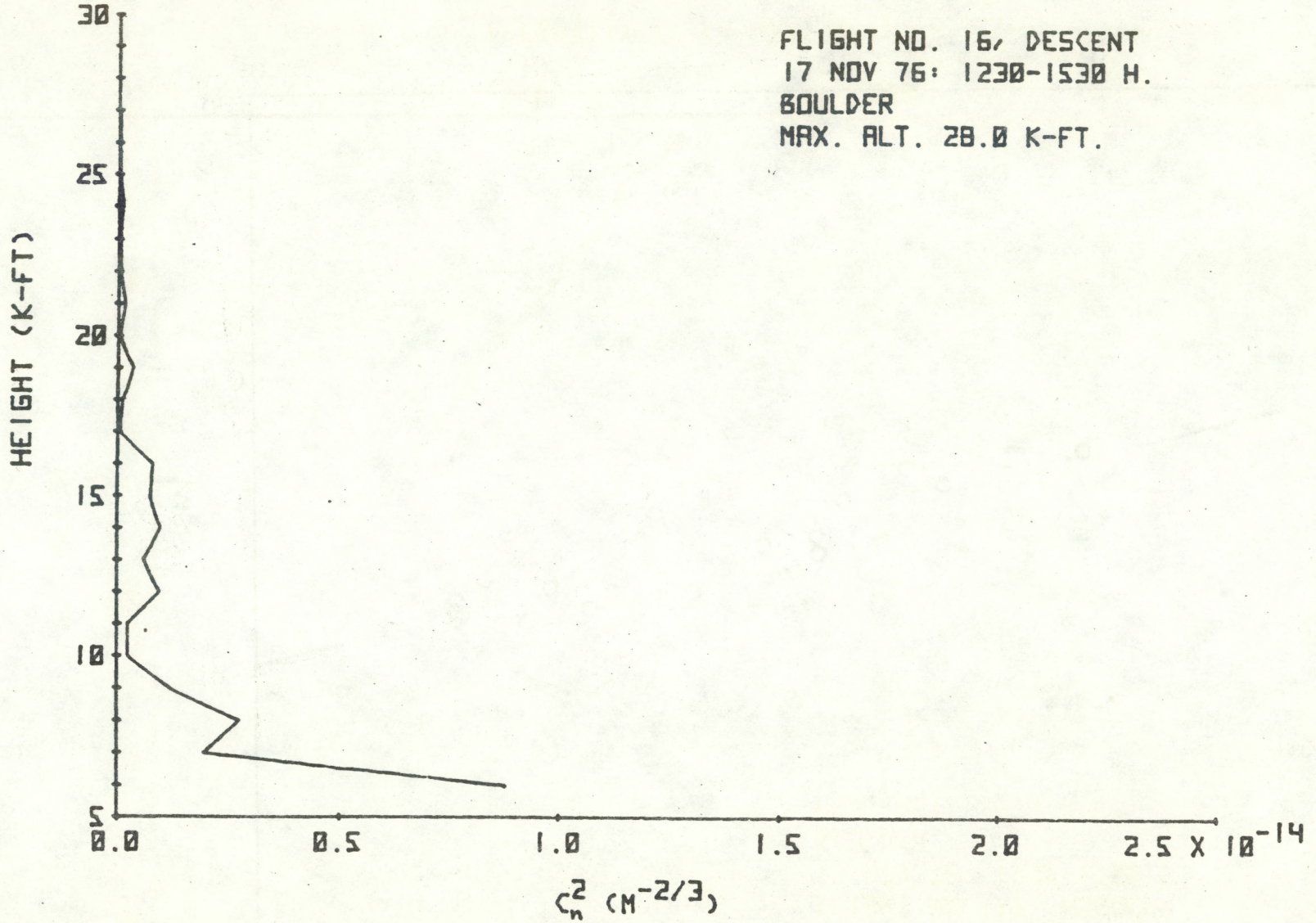

Figure 3-3. C_n^2 sounding corresponding to Figures 3-1 and 3-2.

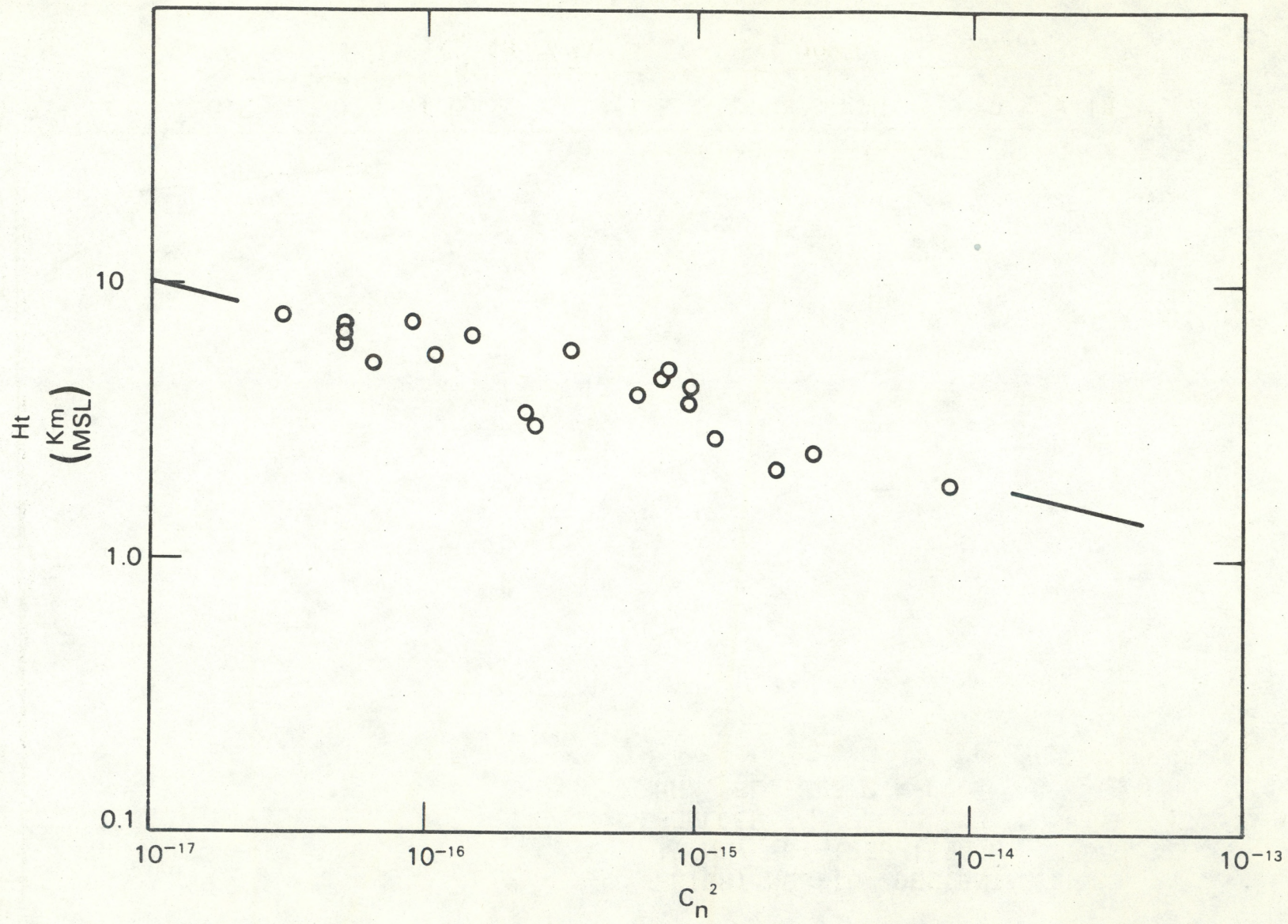

Figure 3-4. Log log plot of C_n^2 vs. height (MSL) corresponding to Figure 3-3.

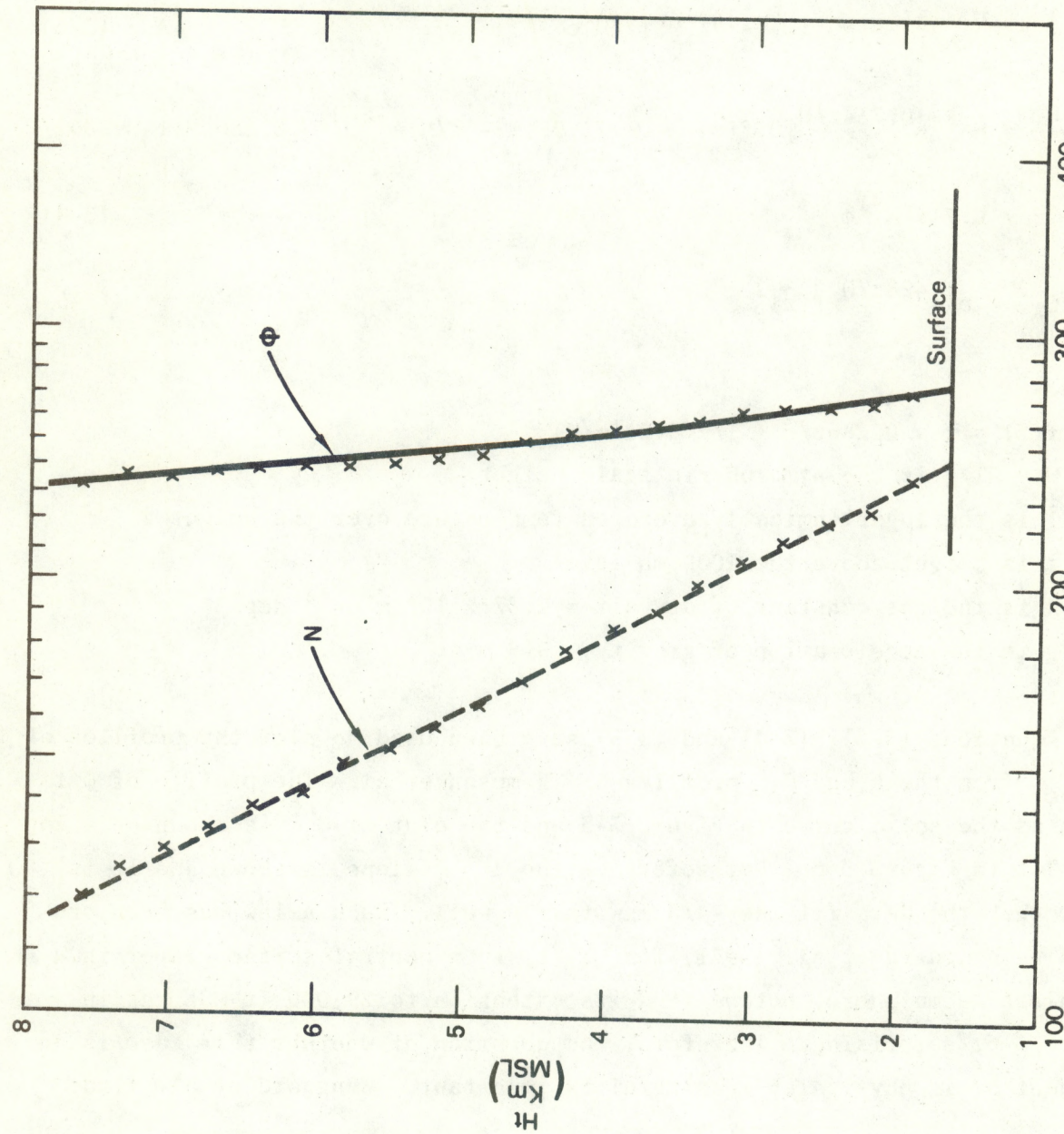

Figure 3-5. Plot of refractive index and potential refractive index vs. height on log paper from data of Figure 3-2.

The measurements of Thompson et al., provide height profiles of N, T and C_n^2. From these quantities we wish to obtain ϕ, C_ϕ^2 and $\partial\phi/\partial z$ as a function of height. The required relationships do not seem to have been published, so we derive them in the Appendix of this paper. We simply state them here:

$$\phi = e^{0.714z/H}[N\ f(z) + 71.95(z/H)e^{-z/H}] \tag{3-3}$$

$$\frac{\partial\phi}{\partial z} = H^{-1}\ e^{0.714z/H}[H\ f(z)\ \frac{\partial N}{\partial z} + 71.95(1 - z/H)e^{-z/H} - 0.286\ N(1-0.286z/H)]$$

$$+ 0.714\ H^{-1}\phi \tag{3-4}$$

$$C_\phi^2 = e^{1.428z/H}\ f(z)^2\ C_n^2 \tag{3-5}$$

where

$f(z) = 1 - 0.286z/H + 1/2(0.286z/H)^2$

$H = R\bar{T}/g$ is the atmospheric scale height

$\bar{T}$ is the logarithmically averaged temperature over the height z

z is height above the 1000 mb level

R is the gas constant of dry air = $2.87 \times 10^2\ m^2\ s^{-1}\ deg^{-1}$

g is the acceleration of gravity = $9.8\ m\ s^{-1}$.

Equations (3-3), (3-4) and (3-5) have been used to plot the profiles of ϕ and C_ϕ^2 from the N and C_n^2 profiles of Thompson et al. The profile of ϕ is shown as the solid curve in Figure 3-5 and the plot of C_ϕ^2 is shown on a log log plot in Figure 3-6. For reference the $z^{-4/3}$ slope is shown and it is clear that the data fit the -4/3 law fairly well. Such a law has been proposed by Wyngaard et al. (1971) for $C_T^2(z)$ in a neutral surface layer in a "windless" atmosphere, but we find its extension to 29,000 ft MSL, as in Figure 3-6, surprising. Therefore, the question of whether this case is an accident or is physically meaningful is important. Wyngaard et al. find:

$$C_T^2 = \frac{4}{3(k_o)^{2/3}} \left(\frac{g}{T}\right)^{-2/3} Q_o^{4/3}\ z^{-4/3} \tag{3-6}$$

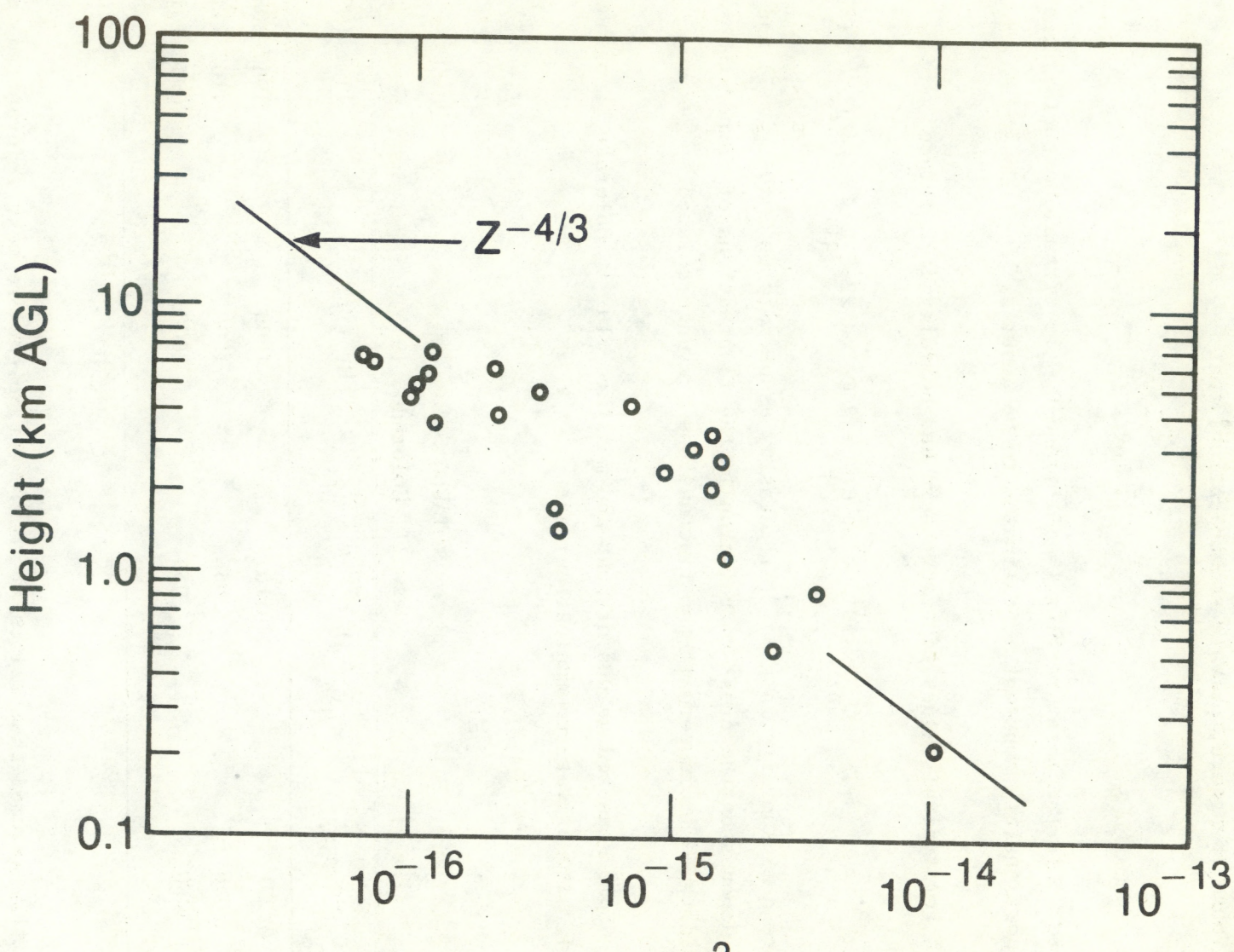

Figure 3-6. Log log plot of C_ϕ^2 vs. height (AGL) corresponding to Figure 3-3. Solid line represents -4/3 power law.

where k_o is Von Karman's constant $\simeq 0.4$, Q_o is vertical heat flux in the surface. Scaling arguments lead to a similar expression for humidity. It is found (Wyngaard, private communication) that

$$C_q^2 \propto M_o^2 \left(\frac{g}{T} Q_{ov}\right)^{-2/3} z^{-4/3} \qquad (3\text{-}7)$$

where M_o is the moisture flux ($= \overline{q'w'}$) and Q_{ov} is virtual heat flux; the proportionality constant is estimated to be about z.

For typical values of temperature and humidity in Colorado

$$C_n^2 \times 10^{12} \simeq 59\, C_q^2 + 2\, C_T^2 - 22\, C_{qT}^2 \qquad (3\text{-}8)$$

where q is humidity in g m^{-3} (air density assumed to be $\sim 10^3$ g m^{-3}) and where C_{qT}^2 depends on the cross correlation in the fluctuations of temperature and humidity — it is zero if the fluctuations are uncorrelated.

Some measured values of heat and moisture flux in Colorado (Lenschow, 1974, also private communication) are

TABLE 3-1

(Haswell, Colorado, 1975)

$\overline{T_v'w'}$ (°C m s^{-1})	$\overline{q'w'}$ (g m^{-3} m s^{-1})	Ht (ft)	Time (MST)
0.27	0.10	1000	1047-1057
.036	.083	1500	1102-1112
.080	.030	2000	0956-1017

If it is assumed that values at the lowest height are most relevant to the surface boundary layer, we might choose $Q_{ov} \simeq 0.3$ and M = 0.1 as representative. Then at a height of 500 ft (1st point in the C_N^2 sounding)

$$C_T^2 = 6 \times 10^{-3}$$

$$C_q^2 = 5.3 \times 10^{-4}$$

so, if the correlation between q and T is assumed to be zero,

$$C_n^2 \simeq 4.3 \times 10^{-14}$$

at 500 ft. If the correlation between temperature and humidity were perfect and negative

$$C_n^2 = 6.2 \times 10^{-14}$$

and if it were perfect and positive

$$C_n^2 = 2.4 \times 10^{-14}.$$

Comparison with the value of C_n^2 at a height of 500 ft in Fig. 3-3 shows that the above calculated values are in very satisfactory agreement with the observed, suggesting that boundary layer transfer processes may indeed be responsible for the -4/3 profile observed on this very well-mixed day.

Case Study of 13 October 1976

Some cases of very regular, well-defined layers were present in the data of Thompson et al., so it was possible to test some of the hypotheses earlier applied to the Ochs-Lawrence data and The PG school data. Such a case was that recorded in Florida on 13 October 1976 between 2100 and 2400. The soundings of temperature, refractive index and C_n^2 are shown in Fig. 3-7, 3-8 and 3-9. As before, various hypotheses were tested for equation (1-3),

$$C_\phi^2 = 2.8\varepsilon^{-1/3} \frac{\overline{w'\phi'}}{\partial z} \frac{\partial \phi}{\partial z}$$

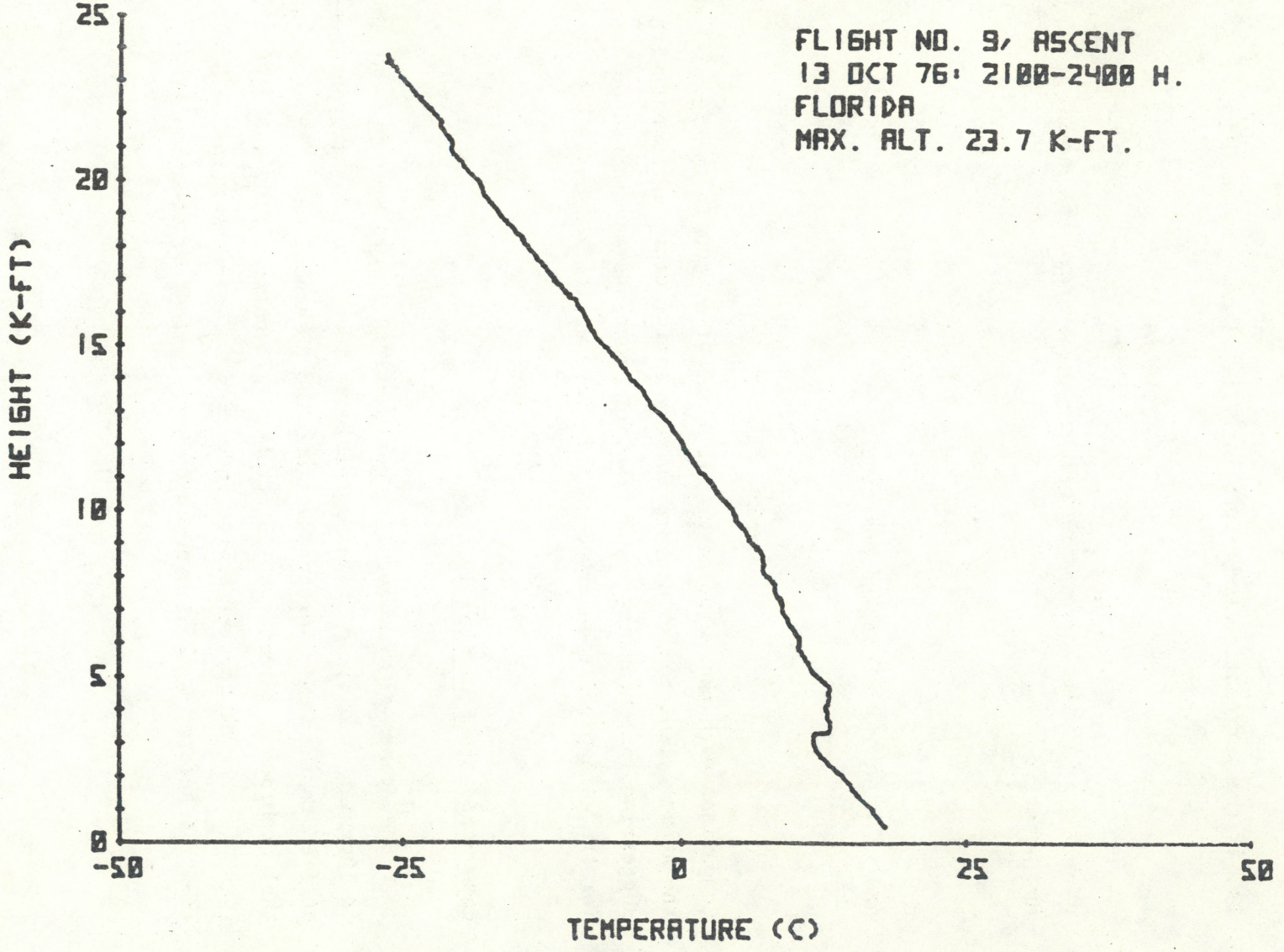

Figure 3-7. Temperature sounding with prominent inversion reported by Thompson et al.

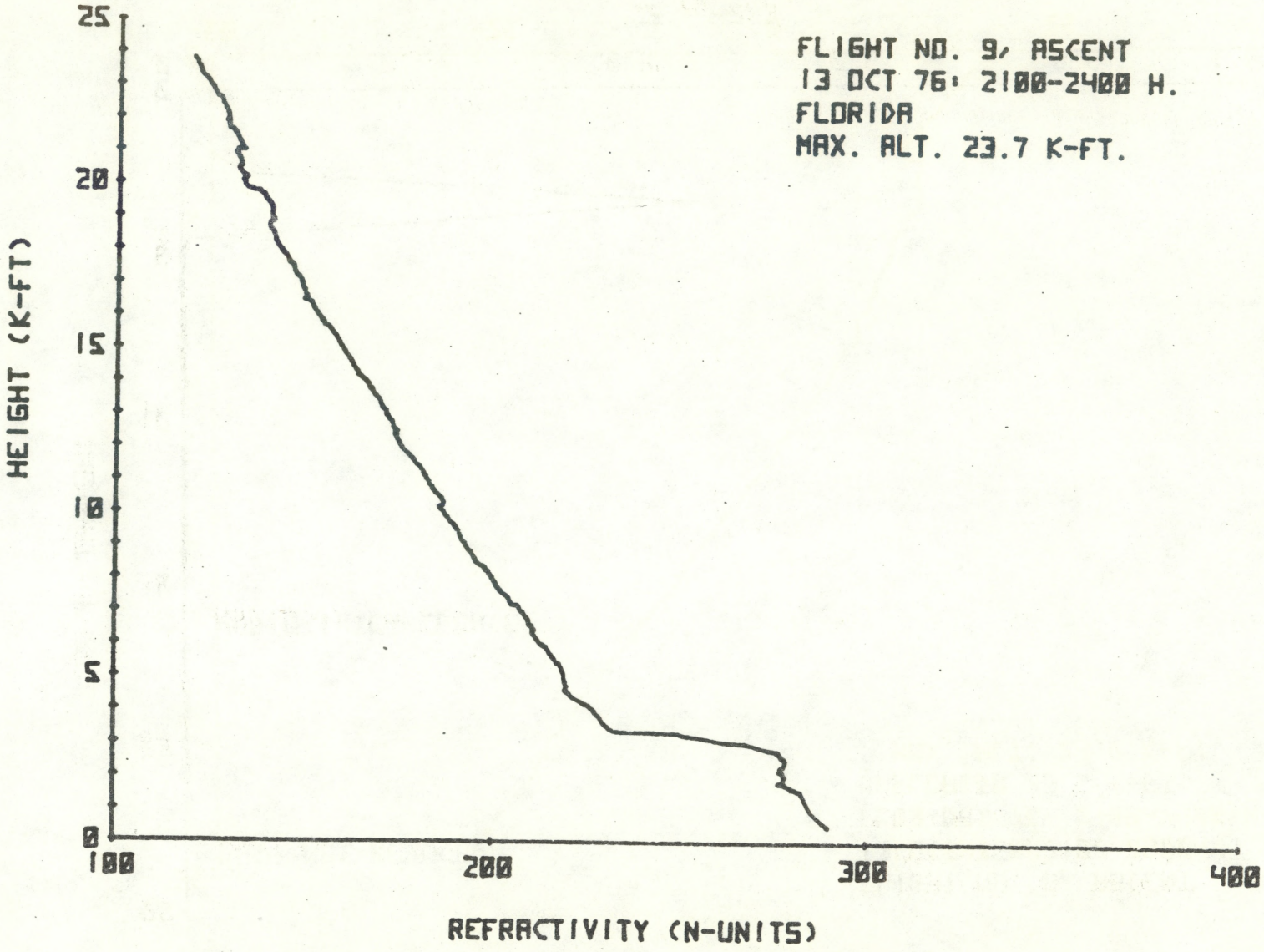

Figure 3-8. Refractive index sounding corresponding to Figure 3-7.

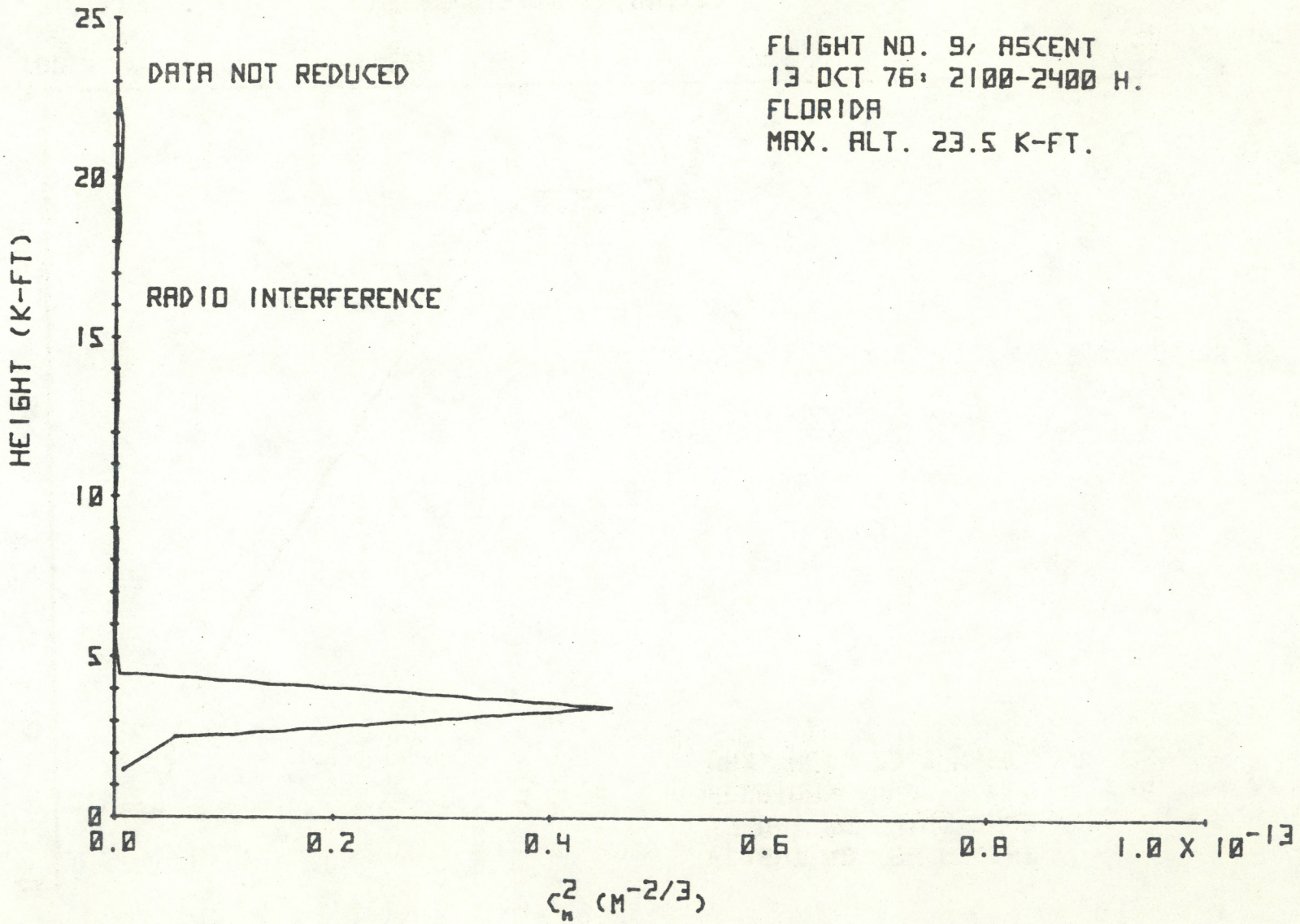

Figure 3-9. C_n^2 sounding corresponding to Figures 3-7 and 3-8.

and the observed gradient was used to try to predict C_ϕ^2 (and therefore C_n^2) and the observed C_n^2 was used to try to predict the profile of ϕ (and therefore N). The results are summarized in Fig. 3-10. The solid curves in the top frame are the observed profiles of C_n^2 (left) and N (right) reported by Thompson et al. The dashed curve on the left is an Epstein Layer "best fit" to the observed distribution in C_n^2. It is shifted slightly in height to match the height of maximum gradient of N. There appears to be a slight lag between the C_n^2 recording and N, but this is trivial in view of the 1000 ft interval digitization of C_n^2.

The lower frame shows (right) a tanh z + az "best fit" to the observed profile of N and the corresponding profile of C_n^2 (left) assuming $\overline{w'\phi'}$ = constant (solid curve) and the eddy coefficient K = constant (dashed curve).

Discussion

Both assumptions apparently underestimate the observed thickness of the C_n^2 layer, but the K = constant assumption underestimates it more seriously than the assumption that $\overline{w'\phi'}$ = constant. The assumption that $C_\phi^2 \propto (\partial\phi/\partial z)^3$ would have produced a C_n^2 layer quite unreasonably thin. Part of the observed "over-thickness" of the layer of C_n^2 may result from smoothing resulting from processing the data over 1000 ft height interval segments, and the comparison of the observed and calculated profiles based on the hypothesis that $\overline{w'\phi'}$ is constant through the layer must be considered to be within experimental uncertainty based on the information available in the report. The "constants" $\overline{w'\phi'}$ or K have, of course, been chosen to match the magnitude of the observed C_n^2. Through relatively thin transition layers, the assumption that $\overline{\phi'w'}$ varies little with height seems to be supported by the data of Thompson et al.

Case Study of 29 April 1976 (Boulder, Colorado) - Chadwick et al. Data Set

Another well documented case for which data were acquired by a very different method, is that of 29 April 1976 from the Boulder-Denver area of Colorado reported by Gossard et al. (1978). The structure parameter of

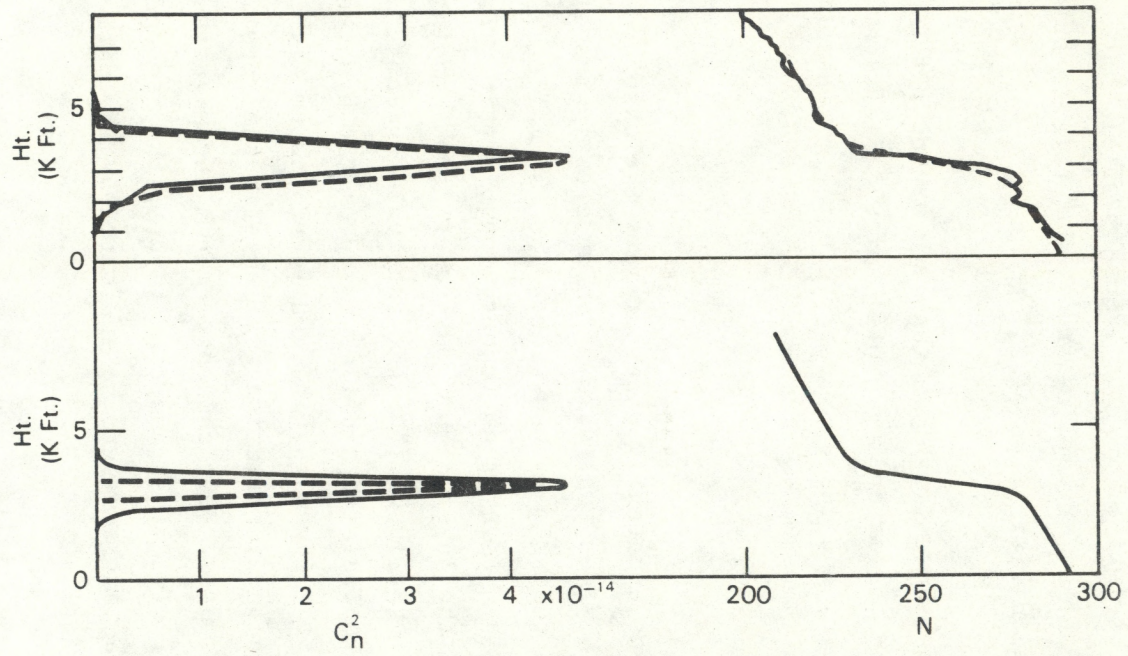

Figure 3-10. Top frame: Observed data (solid curves) for case of Figures 3-8 and 3-9. The dashed curve is an Epstein Layer "best fit" to the observed distribution in C_n^2 shifted slightly to match the height of maximum gradient of N, Lower frame: A tank z + az "best fit" to the observed profile of N (right) and the corresponding profile of C_n^2 (left) assuming $\overline{W'\phi'}$ = constant (solid curve) and eddy coeffecient K = constant (dashed curve).

radar refractive index C_n^2 was remotely sensed by a vertically pointing FM-CW radar, and the height distribution of turbulent dissipation rate ε was calculated from the width of the radar Doppler velocity spectrum. Samples of the radar records and the calculated profiles are shown in Figs. 3-11 and 3-12. The temperature, humidity, and wind-sounding data were obtained from the Denver RAWIN about 5 hours before the Boulder radar observations. The weather situation was remarkably stable, and the elevated layer resulted from a nearly stationary frontal system lying along the eastern edge of the Colorado Rocky Mountains. The profiles of potential temperature θ and potential refractive index ϕ are shown in Fig. 3-13 as plotted from the raob data.

In Fig. 3-14 (lower frame) two profiles of $C_n^2 = C_\phi^2$ are shown taken about a half hour apart. The dashed profile was acquired in the Doppler mode of operation and had a height resolution of 80 m. The solid curve profile was acquired in a range-only mode with a height resolution of 6 m. In the upper frame of the figure C_n^2 is shown on an expanded height scale and a smooth dashed curve has been drawn thru the range only profile. These curves were used to read the interpolated values of C_n^2 for intermediate height levels.

Figure 3-15 shows the values of potential refractive index gradient $d\phi/dz$ from the RAWIN data (step profile). The profiles from the RAWIN are necessarily coarse and consist of layers of constant gradient because of the methods used in working up standard raob soundings. An Epstein profile imbedded in a standard refractive index profile gradient ($.013\ m^{-1}$) has been arbitrarily fitted to the raob data as indicated by the two smooth curves. The solid curve is fitted to the Doppler radar $C_n^2 \equiv C_\phi^2$ data taking 60 m as the scale thickness of the layer and taking $\Delta\phi = 25 \times 10^{-6}$ across the layer. The dashed curve is fitted to the range-only radar C_ϕ^2 data taking 80 m as the scale thickness and $\Delta\phi = 25 \times 10^{-6}$ across the layer. If we now use the data from the top frame of Fig. 3-14 and the smooth profiles from Fig. 3-15, the distribution of flux $w'\phi'$, K, and $\frac{\Delta u}{\Delta\phi} L^2$ can be calculated. Assuming $\varepsilon = 1$, the results are shown in Table 3-2. In Table 3-2 the Denver raob data have been shifted downward 110 m so that the height of maximum gradient matches the height of the maximum C_ϕ^2 measured by the radar. The height difference

Sample of radar record used to calculate C_n^2. Left frame: Backscattered intensity vs. height and time. Right frame: A scope display of power vs. height and Doppler wind spectra vs. height. Spectra are centered on zero frequency shift because radar is pointing vertically; range (height) ϕ ins 87 m wide.

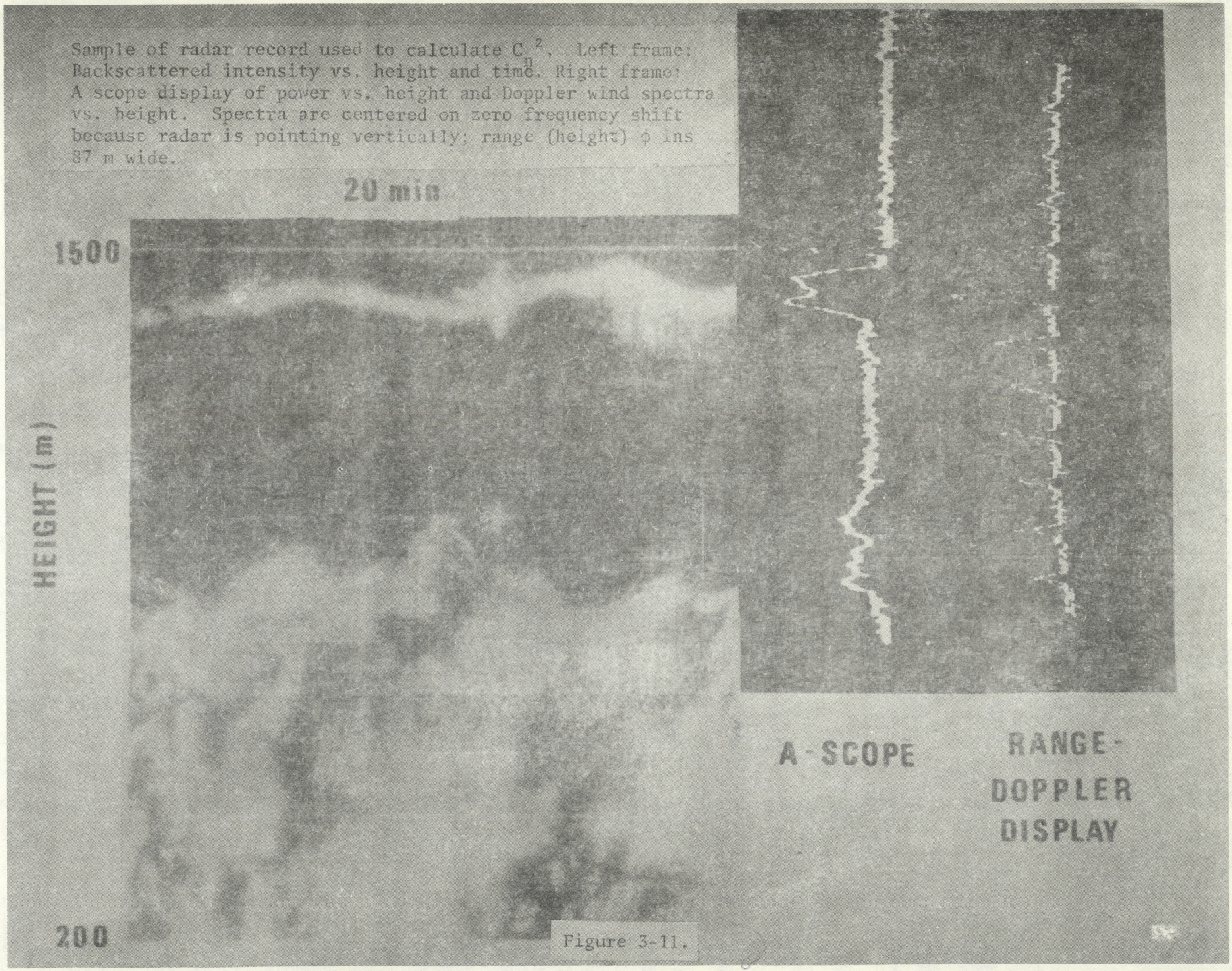

Figure 3-11.

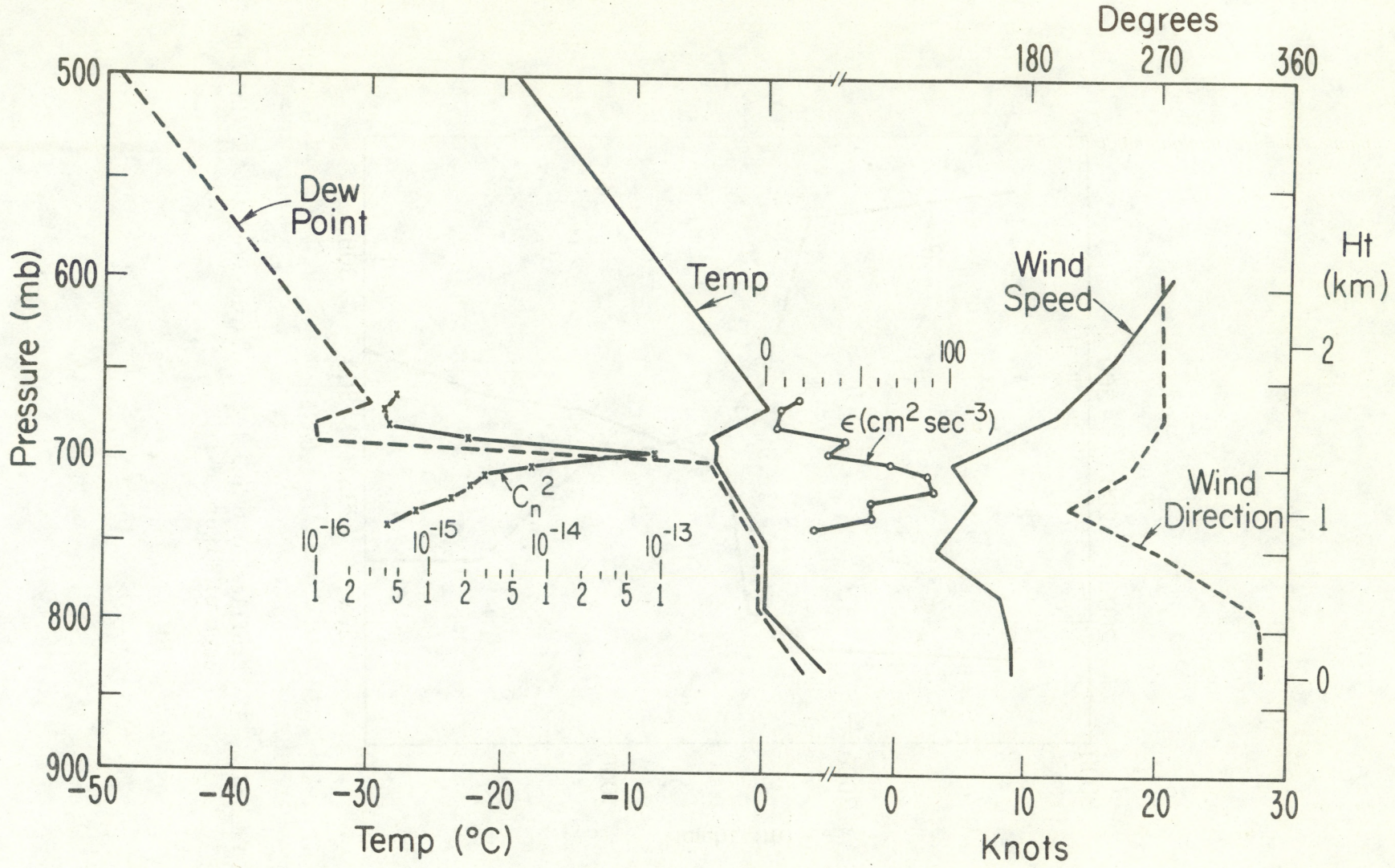

Figure 3-12. Denver RAWINSONDE sounding data corresponding to record in Figure 3-11 with C_n^2 and ε calculated from the radar data.

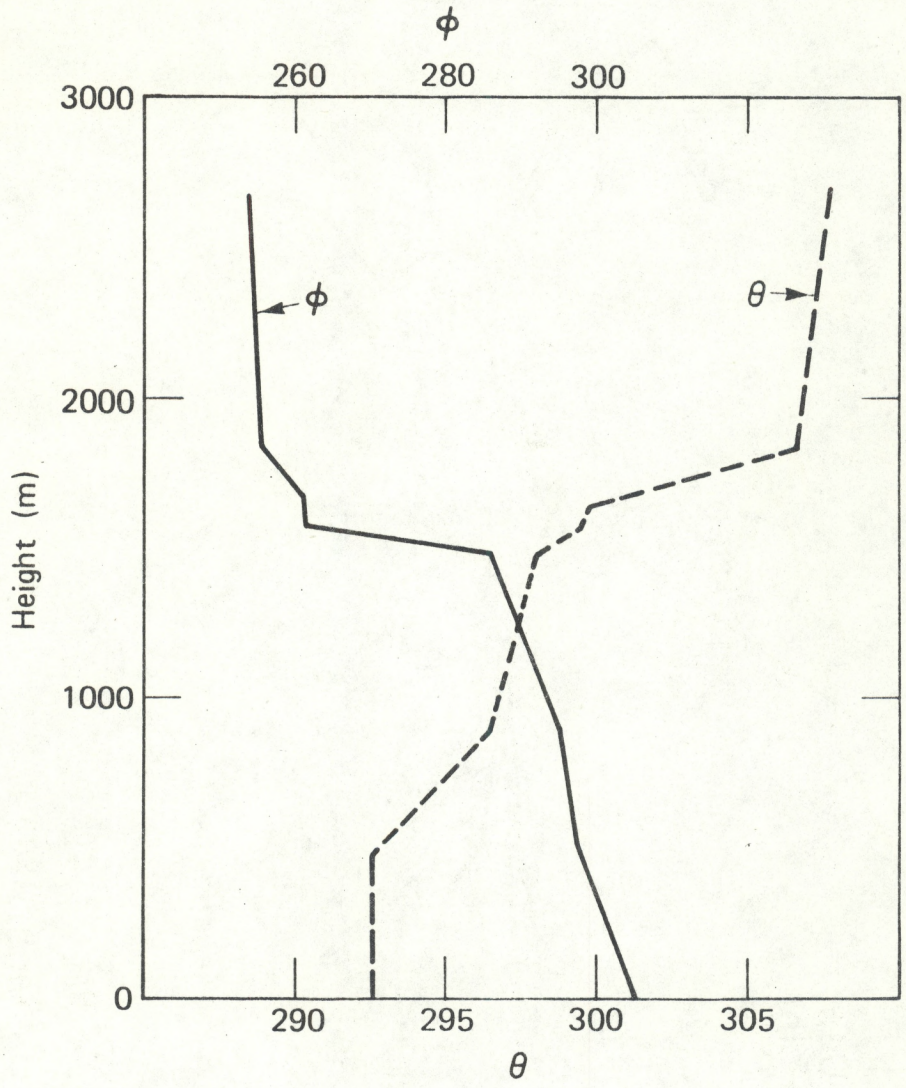

Figure 3-13. Profiles of 0 and ϕ calculated from the RAWINSONDE data of Figure 3-12.

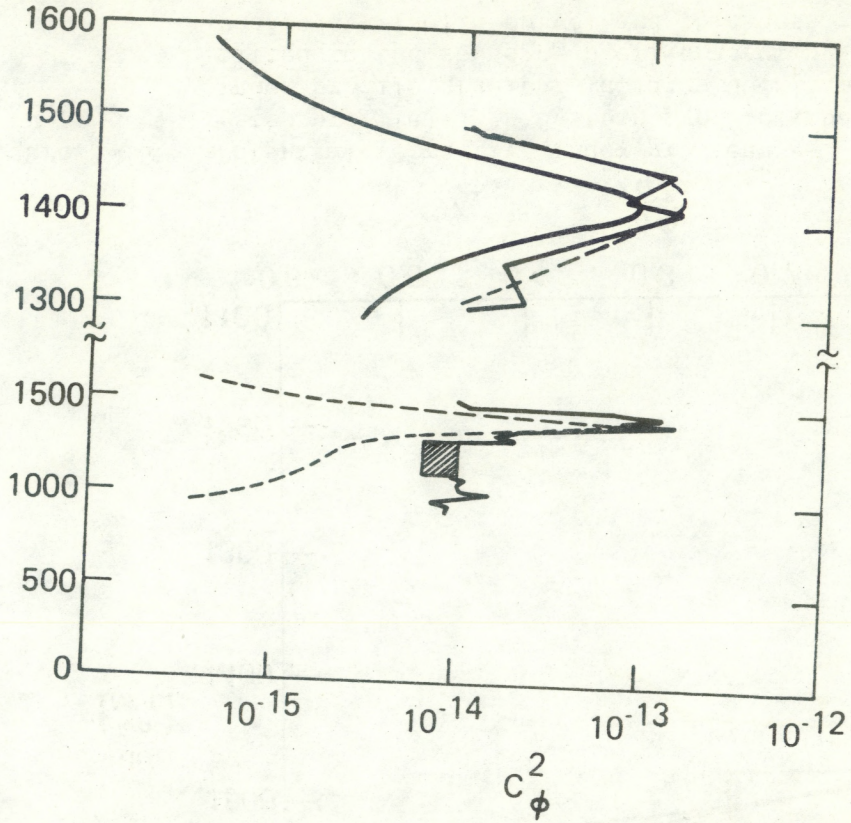

Figure 3-14. Lower frame: Profiles of C_n^2 calculated from Doppler spectra (dashed curve) and from backscattered power (solid curve). Upper frame: Two solid curves are the same as lower frame on expanded height scale. Dashed curve is smoothed profile used for interpolation of non-Doppler C_n^2.

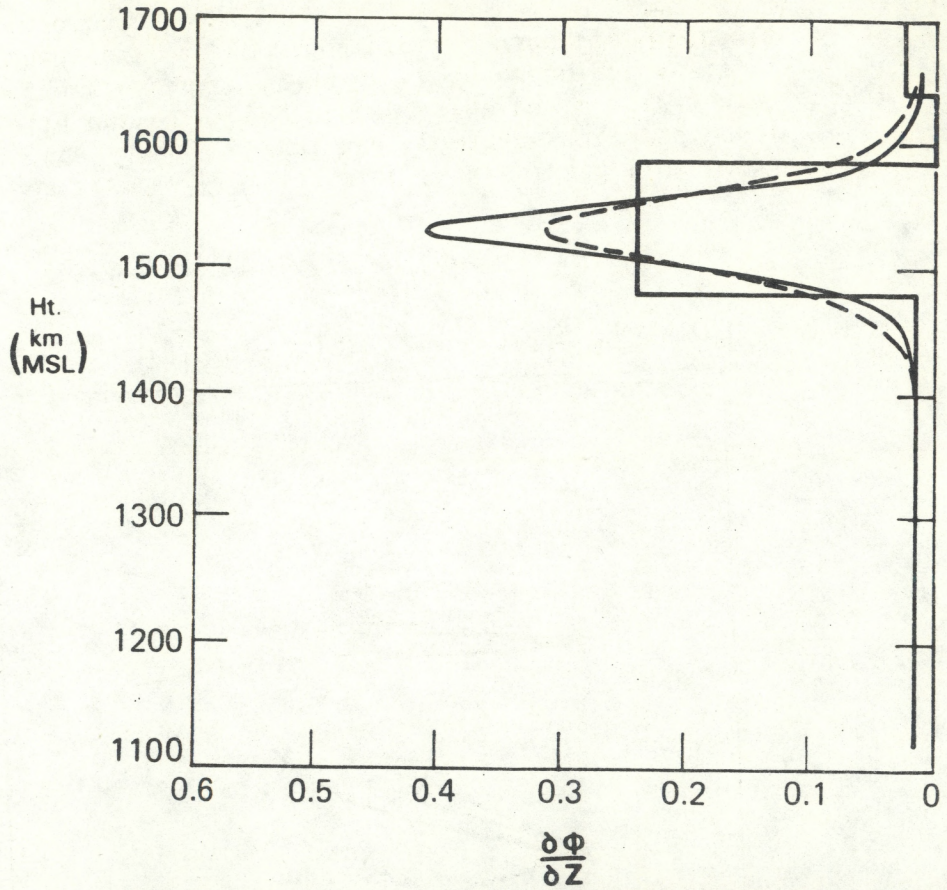

Figure 3-15. Potential refractive index gradient vs. height from RAWINSONDE data (step profile). An Epstein profile imbedded in a standard refractive index profile gradient ($d\phi/dz$ = 00.013 m^{-1}) has been arbitrarily fitted to the sounding profile assuming thickness = 60 m from Doppler radar data (solid curve) and thickness = 80 m from non-Doppler data (dashed curve). Both cases assume a total change in ϕ across the layer of 25 x 10^{-6}.

TABLE 3-2

Radar in Doppler Mode (h=60m, ${}_oC_\phi{}^2=8.5\times10^{-14}$)

Ht (m)	Flux	K	$\frac{\Delta u}{\Delta\phi} L^2$
1350	9.6×10^{-8}	3.5	1.25×10^{8}
1370	7.6×10^{-8}	1.1	1.7×10^{7}
1390	7.9×10^{-8}	0.44	2.4×10^{6}
1410	7.7×10^{-8}	0.21	5.6×10^{5}
1430	6.7×10^{-8}	0.18	4.9×10^{5}
1450	4.9×10^{-8}	0.27	1.5×10^{6}
1470	4.3×10^{-8}	0.65	9.8×10^{6}
1490	3.9×10^{-8}	1.4	5.0×10^{7}

Radar in Range-Only Mode (h=50m, ${}_oC_\phi{}^2=1.5\times10^{-13}$)

Ht (m)	Flux	K	$\frac{\Delta u}{\Delta\phi} L^2$
1350	2.3×10^{-7}	4.8	1.0×10^{8}
1370	1.8×10^{-7}	1.9	1.9×10^{7}
1390	1.5×10^{-7}	0.78	4.0×10^{6}
1410	1.6×10^{-7}	0.53	1.8×10^{6}
1430	1.8×10^{-7}	0.61	2.1×10^{6}
1450	1.9×10^{-7}	0.97	5.0×10^{6}
1470	1.8×10^{-7}	1.9	1.9×10^{7}
1490	1.1×10^{-7}	2.4	5.1×10^{7}

of Boulder and Denver can account for 40 m of the discrepancy; the 5 hour time displacement and 60 km spatial displacement can reasonably account for the remainder.

As in the San Diego subsidence inversion case of 5 October, the flux seems to be much more constant than either K of $(\Delta u/\Delta\phi)L^2$ and, in fact, is

probably constant within the error bounds introduced by the crudeness of the raob sounding. However, as in the subsidence inversion case, there seems to be a tendency for the flux to increase downward. Appearing in both cases, it is probably significant. The possible interpretation of such a trend will be discussed later.

4. STATISTICS OF OCCURRENCE OF REFRACTIVE LAYER STRUCTURE

Thompson et al. Data Set

In the measurements reported by Thompson et al., profiles up to 29,000 ft were obtained near Boulder, Colorado and in Florida. Some statistics of their observations are compiled in Table 4-1.

TABLE 4-1

Radio C_n^2 from Microwave Refractometer (Thompson et al., 1977)
(Statistical Compilation)

Boulder Flt No.	Max C_n^2	Min C_n^2	Ht Max (K ft)	Ht Min (K ft)	Top Sndng	C_n^2 at Top
2Ascent(Sept.'76)	1.01×10^{-13}	3.50×10^{-16}	8.5	11.5	12.5	3.8×10^{-15}
3A	1.68×10^{-14}	1.24×10^{-16}	5.5	12.5	12.5	1.2×10^{-16}
4Descent	1.21×10^{-13}	7.60×10^{-17}	7.5	11.5	11.5	7.6×10^{-17}
5A	2.49×10^{-13}	5.98×10^{-17}	7.5	11.5	12.5	6.6×10^{-16}
5D	6.77×10^{-14}	4.13×10^{-17}	7.5	11.5	12.5	3.4×10^{-16}
15A (Nov.'76)	7.13×10^{-15}	2.59×10^{-17}	7.5	26.5	27.5	5×10^{-17}
15D	1.03×10^{-14}	2.98×10^{-17}	8.5	27.5	28.5	5×10^{-17}
16A	8.93×10^{-15}	3.39×10^{-17}	10.0	27.0	27.0	3.4×10^{-17}
16D	8.78×10^{-15}	2.84×10^{-17}	6.0	26.0	27.0	3.4×10^{-17}
17A	3.44×10^{-15}	3.19×10^{-17}	6.0	28.0	28.0	3.2×10^{-17}

TABLE 4-1 (continued)

Radio C_n^2 from Microwave Refractometer (Thompson et al., 1977)

(Statistical Compilation)

Florida

Flt No. (Oct.'76)	Max C_n^2	Min C_n^2	Ht Max (K ft)	Ht Min (K ft)	Top Sndng	C_n^2 at Top
6A (Rain)	1.21×10^{-13}	3.93×10^{-17}	5.5	20.5	20.5	3.9×10^{-17}
6D (Rain)	1.11×10^{-13}	1.61×10^{-16}	13.0	18.5	20.5	5.1×10^{-16}
7A	1.92×10^{-13}	3.39×10^{-17}	0.5	19.5	22.5	4.6×10^{-17}
7D	2.65×10^{-13}	1.76×10^{-17}	4.0	17.5	23.0	4.6×10^{-17}
8A	7.36×10^{-14}	2.61×10^{-17}	4.5	18.5	22.5	2.6×10^{-17}
8D	1.01×10^{-13}	2.68×10^{-17}	2.0	18.0	18.0	2.7×10^{-17}
9A	4.58×10^{-14}	3.09×10^{-17}	3.5	15.0	22.5	1.8×10^{-16}
9D	4.79×10^{-15}	2.89×10^{-17}	3.5	13.5	23.5	7.5×10^{-17}
10A	6.15×10^{-14}	2.61×10^{-17}	0.5	10.5	23.5	3.5×10^{-17}
10D	1.52×10^{-13}	2.92×10^{-17}	0.5	6.5	21.5	1.4×10^{-16}
11A	2.62×10^{-13}	2.19×10^{-17}	0.5	24.5	24.5	2.2×10^{-17}
11D	2.17×10^{-13}	2.25×10^{-17}	6.5	22.5	24.5	3.0×10^{-17}
12A	9.59×10^{-14}	2.35×10^{-17}	0.5	23.5	24.5	2.4×10^{-17}
12D (Rain)	4.04×10^{-13}	1.73×10^{-17}	5.5	20.5	24.5	2.6×10^{-17}
13A (Rain)	1.22×10^{-13}	1.38×10^{-17}	2.5	17.5	24.5	2.7×10^{-17}
13D (Rain)	5.72×10^{-14}	1.07×10^{-17}	1.5	19.5	24.5	2.6×10^{-17}
14A (Clouds)	4.82×10^{-14}	2.02×10^{-17}	4.5	21.5	24.5	5.8×10^{-17}
14D	8.27×10^{-14}	2.60×10^{-17}	3.5	19.5	24.5	9.6×10^{-17}

If radar reflections are to be used as an indicator of temperature inversions, the prediction failure rate is important. Thus the percentage of time when an inversion (or layer of significant temperature stability) was not accompanied by a spike in C_n^2 is of interest.

At Boulder there were no cases when temperature inversions were not accompanied by spikes in C_n^2. The Boulder data included 11 soundings over 7 days in September

and November. There were a total of 13 inversion layers in the soundings and 15 super-refractive layers.

In Florida, there were 7 inversion layers on 3 days that were not accompanied by C_n^2 spikes. The Florida data included 18 soundings over 9 days in October. There were 38 inversion layers and 34 super refractive layers. Thus in Florida a failure rate of 18% is indicated based on layer number.

For the inverse case of "false alarms" due to the presence of a C_n^2 spike unaccompanied by temperature inversions, 2 such cases (out of 13 inversion layers) occurred at Boulder; one case was unaccompanied by a super-refractive layer. Thus, for temperature at Boulder, a false alarm rate of 15% is indicated.

In Florida 3 false alarms (out of 38 inversions) were measured, all on different days. Three spikes of C_n^2, all on different days, were unaccompanied by super-refractive layers out of a total of 34 super-refractive layers. Thus a false alarm rate for temperature inversions (or significantly stable layers) in Florida was about 8%. It is to be emphasized that there is a great deal of subjectivity in deciding what is a "significant" spike, stable layer, or super-refractive layer. Only radar statistics will be ultimately decisive.

A few additional points are worth noting:

A) The vast majority of super-refractive layers in both Boulder and Florida were accompanied by temperature inversions and vice versa. Only one layer (out of 15) in Boulder and 5 layers (out of 34) in Florida were not accompanied by temperature inversions. Thus, detection of a significant super-refractive layer would carry a strong implication of a temperature inversion. Apparently moisture gradients are usually accompanied by temperature inversions and vice versa.

B) The difference in soundings on ascent and descent was very great — in some cases almost as great as day-to-day variability. Thus, the

ascent at Boulder on 17 November showed 3 inversions accompanied by 3 super-refractive layers and a significant spike in C_n^2 at 10,000 ft, whereas the descent profiles indicated a remarkably homogeneous atmosphere. This suggests that local temporal and spatial variability may provide a large percentage at the "noise" in the process of extracting representative soundings. This in turn suggests that the ability of remote sensors to monitor temporal patterns continuously and average out temporal (and by implication spatial) variability may be of great importance. The cases of false alarm or failure to detect may be eliminated by averaging out the horizontal spatial variability.

C) The common occurrence of sub-refractive layers in Florida is interesting. Such layers occurred in 6 out of 18 soundings. If real, these layers imply an increase in moisture with height through a thin transitional region. They were usually accompanied by an adiabatic temperature lapse. The implication is that moist, cool air lies above dryer relatively warm air — an unstable situation that usually produced large C_n^2 spikes. Such a situation should be fairly transient, but it was often noted on both ascent and descent over time intervals of 4 hours. The soundings at 14 October and 15 October were especially convincing and reproducible on descent. The soundings of 16 October and 18 October also provided excellent, persistant examples of sub-refractive layers. However, rain occurred on these days and anomalous effects on the refractometer cavity cannot be ruled out, although no rain was reported during ascent on 16 October when several sub-refractive layers were reported. A common explanation for such subrefraction is local horizontal inhomogeneity over the path of the aircraft, but its reproducibility in height for both ascent and descent seems to rule out such an explanation. The gradients are often so large as to be very puzzling.

5. USE OF CHANGE IN LAYER HEIGHT TO DEDUCE FLUX INFORMATION

Most of the data analyzed in this report suggest that the layers observed were in approximate steady state. If temporal change is occurring the flux

will not be constant with height across the layer. A simple way of expressing the rate of change in height in terms of the change in flux across the layer is provided by the "flux integral" technique Gossard (1953). The rigorous solution is replaced by an approximate method that treats the time-changing part of the problem as a change in height of the transition layer while ignoring the fairly minor changes in the functional form of the profile above and below the layer of transition. For comparison of the approximate method with special rigorous solutions of diffusion problems see Gossard (1978). In this method the difference in vertical flux across a layer is equated to the time rate-of-change of the total heat (or moisture) in the blanket below the height $\delta(t)$ of transition (see sketch).

Thus, for heat;

$$\rho C_p \frac{d}{dt} \int_o^{(t)} (\theta_\delta - \theta_2)\, dz = - \Delta F \qquad (5\text{-}1)$$

where θ_δ is potential temperature at height δ and ΔF is flux above minus flux below the transition.

Suppose the transition layer has the hyperbolic tangent functional form. Then

$$\theta_z - \theta_s = (\theta_\delta - \theta_s)(\tanh \frac{z-\delta}{h} + 1) \qquad (5\text{-}2)$$

where h is transition layer thickness. Substituting (5-2) into (5-1) and integrating, we readily find that

$$\frac{d}{dt} [(\theta_\delta - \theta_s) \log \cosh (-\frac{\delta}{h})] = - \frac{\Delta F}{\rho C_p} \qquad (5\text{-}3)$$

When the transition layer is very thin ($h \to 0$) and equation (5-3) takes the especially simple form

$$\frac{d(\theta_\delta - \theta_s)\delta}{dt} = - \frac{\Delta F}{\rho C_p} \cdot \qquad (5\text{-}4)$$

Thus, for a system in which $\theta_\delta - \theta_s$ remains approximately constant in time, the rate of change in layer height can be used to infer the flux change across the layer and the flow of heat into or out of the lower region. If downward flux decreases downward through the layer, the layer will move downwards. If downward flux increases downward through the layer, the layer will move upwards. Thus change in layer height may be used to deduce height gradient in flux thru the layer providing a correction to the steady state model.

6. PROPOSED MODEL RELATING C_n^2 TO REFRACTIVE INDEX GRADIENT

The data analyzed in this report suggest that the assumption that $\overline{w'\phi'}$ is approximately constant in elevated, stably stratified layers is valid under steady-state conditions. However, there is some tendency for a decrease

of apparent flux with height, if only the 1st term on the right side of equation (1-2) is assumed to be important, as in the example shown in Table (2-1).

There is a general decrease in background C_n^2 with height that can be approximated by a power law. The case of 18 October 1976 reported by Thompson et al. (1977) suggests that the power is very nearly -4/3 for C_ϕ^2 when the atmosphere is well-mixed and homogeneous.

These results suggest a model with layers (in which C_ϕ^2 varies approximately proportionally to $d\phi/dz$) superimposed on a background distribution for which C_ϕ^2 decreases according to a power of height. Thus we might try a model such that

$$C_\phi^2 = [a + c \sum_{i=1}^{i=N} \frac{\Delta\phi_i}{h_i} \operatorname{sech}^2 \frac{z-H_i}{h_i}] z^{-b} \qquad (6\text{-}1)$$

where a, b and c are free constants to be determined from radiometric retrieval or from climatology. The height gradient of ϕ has been assumed to be of Epstein form so

$$\frac{d\phi}{dz} = \frac{\Delta\phi}{h} \operatorname{sech}^2 \frac{z-H}{h} \qquad (6\text{-}2)$$

where z is height, h is layer thickness, H is layer height and $\Delta\phi$ is the change in ϕ across the elevated layer. The summation is over N layers, i = 1,2,3 ... N. If equation (6-1) is shown to be an accurate representation, it can, of course, be inverted to obtain $d\phi/dz$ (and therefore ϕ) from measurements of C_ϕ^2 made with radars. Such an inversion would be done numerically because there apparently is no expression for the inversion in terms of elementary functions.

To test the usefulness of equation (6-1) the sounding data of Thompson et al. (1977) for 18 October 1976 in Florida have been used. The ascent and

descent profiles of N are shown in Figure 6-1. Using equation (8A), the profiles of N and C_n^2 are readily converted to profiles of ϕ and C_ϕ^2 and back again. Four significant layers were picked off the profiles as shown in Table 6-1.

TABLE 6-1

H (ft)	$\Delta\phi$	h (ft)
2000	20	100
5300	30	500
6900	5	100
10500	2	100

Using equation 6-1 and (5A), the height distribution of C_n^2 is readily calculated and is shown plotted (dashed curve) in Figure (6-2) along with the profiles of C_n^2 observed on ascent and descent (solid curves). In the calculation, a was chosen to be 10^{-14}, b was -4/3 and c was 5×10^{-17}. The quantity C_n^2 is obviously very volatile and varies a great deal between ascent and descent, but the resemblance to the calculated profile is unmistakable. Obviously if the calculated profile were properly inverted, it would lead to a profile of ϕ with the layer characteristics of that described by Table 6-1. It therefore seems probable with suitable averaging (perhaps over an hour) such as is possible with a radar, that the inversion of such a C_n^2 profile would lead to a reliable estimate of the profile of ϕ, and therefore of N.

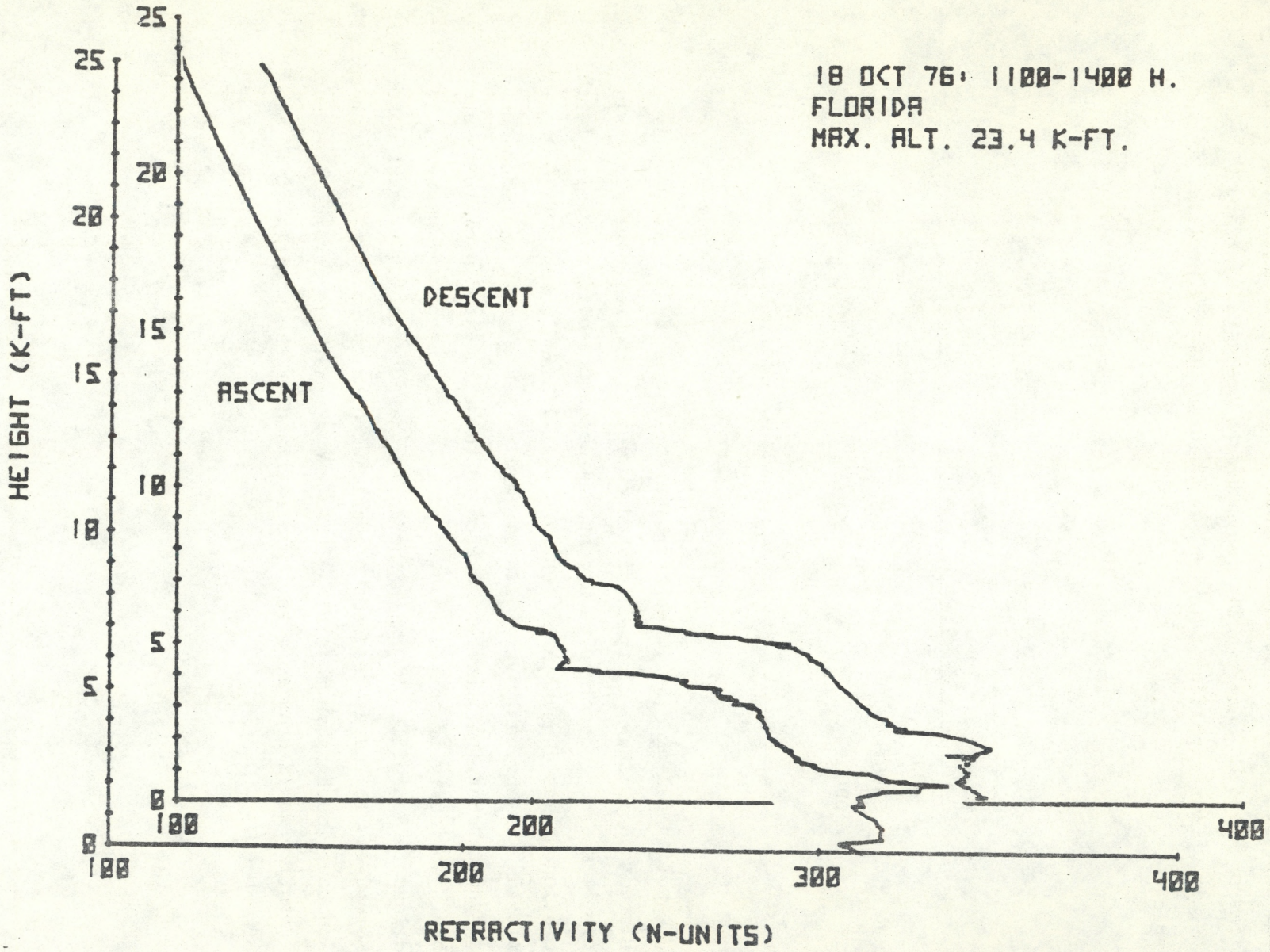

Figure 6-1. Refractive index profiles measured by Thompson et al. on a day when there were several refractive layers.

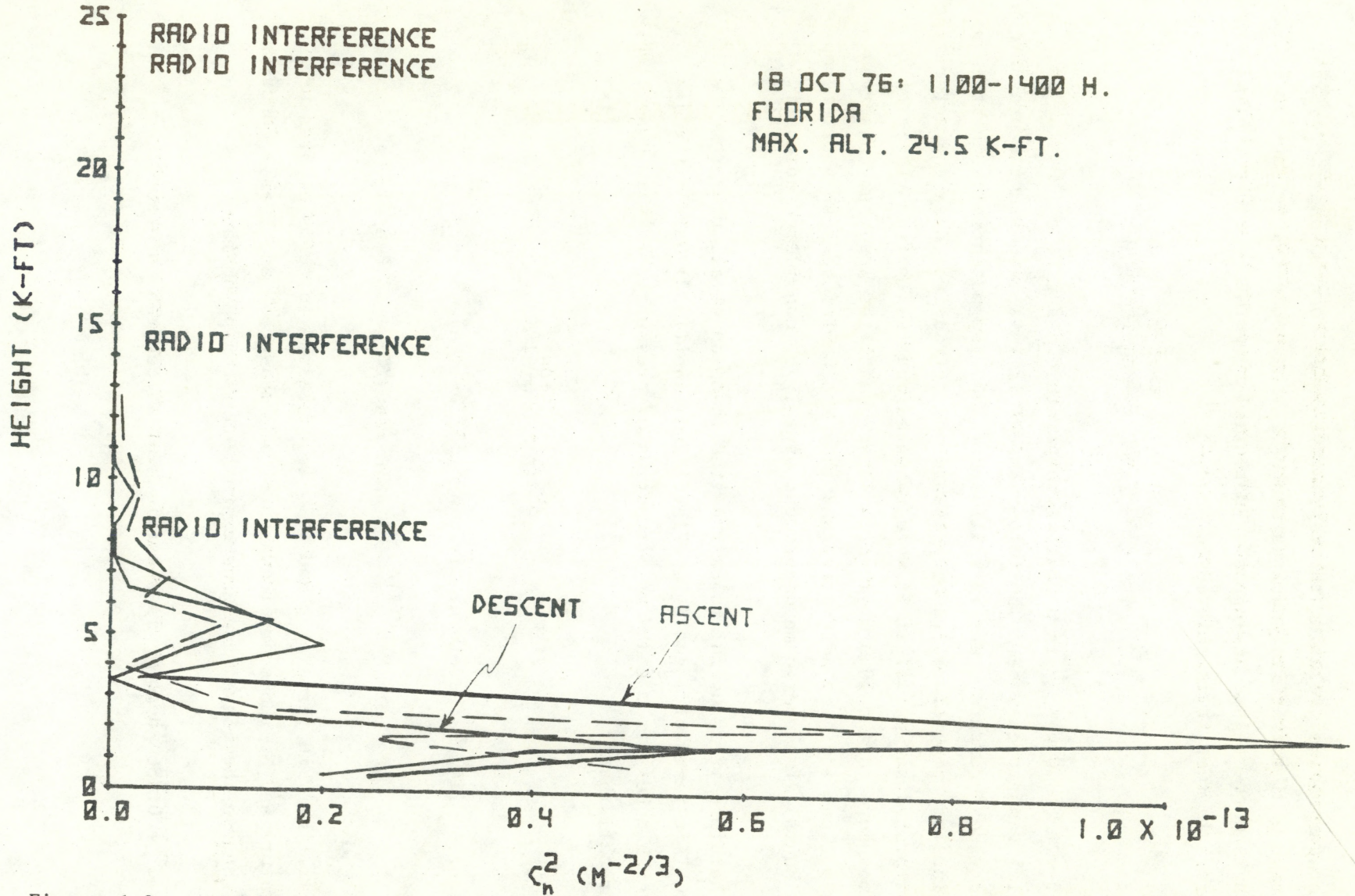

Figure 6-2. Solid curves are measured profiles of C_n^2 for the R.I. profiles shown in Figure 6-1. The dashed curve is the distribution of C_n^2 that would have been calculated from a four layer model representative of that shown in Figure 6-1 and calculated from Equation (6-1) choosing $a = 10^{-14}$, $b = -4/3$ and $c = 5 \times 10^{-17}$. The assumed layer characteristics are given in Table 6-1. The calculated dashed curve is a good representation of the average of the profiles observed on ascent and descent.

APPENDIX

RADIO POTENTIAL REFRACTIVE INDEX

For purposes of relating the refractive index to atmospheric physics, the most useful refractive index parameter is the potential refractive index ϕ which is more-or-less analogous to potential temperature and potential vapor pressure. In fact it is related to them as

$$\phi = \frac{77.6}{\theta}\left(1000 + \frac{4810\, e_p}{\theta}\right) \qquad (1A)$$

where $\theta = T\,(1000/p)^{R/C_p}$ is potential temperature and $e_p = e\,(1000/p)$ is potential vapor pressure*. The temperature T is in Kelvin and the pressure p and the vapor pressure e are in millibars. Thus the potential quantities are the values of temperature, vapor pressure and refractive index characterizing an unsaturated air parcel if it were taken adiabatically from its level in the atmosphere to the 1000 mb level. These quantities are thus conserved during motions that are adiabatic, and they are useful because short-term (a few hours) atmospheric movements can usually be considered adiabatic.

Therefore it is useful to express the Thompson et al. measurements of N and C_n^2 in terms of ϕ and C_ϕ^2. Flavel and Lane (1962) have derived a relationship between ϕ and N as a function of pressure. This is done simply if we recall that

$$N = \frac{77.6}{T}\left(p + \frac{4810e}{T}\right) \qquad (2A)$$

analogous to (1A). Therefore, dividing (1A) by (2A)

$$\phi = N\, e^{0.714}(1 + 4810\, e/p\theta)/(1 + 4810\, e/pT). \qquad (3A)$$

Then, writing θ in terms of p and T, ϕ is expressed in terms of pressure, temperature and N. However, Thompson et al. measure N and T as a function of <u>height</u>, so the Flavel and Lane expression is inappropriate.

---

* $R/C_p = 0.286$ where C_p is specific heat at constant pressure.

However writing the denominator of (3A) as TN/77.6 it is evident that

$$\phi = \left(\frac{1000}{p}\right)^{.714} \frac{77.6}{T} \left[p + \frac{4810\ e}{T} \left(\frac{1000}{p}\right)^{-.286}\right].$$

Combining the hydrostatic equation,

$$dp = - \rho g\, dz \tag{4A}$$

with the equation of state,

$$\rho = \frac{p}{RT} \tag{5A}$$

where ρ is density, $g = 9.8\ m\ s^{-2}$ is gravitational acceleration and $R = 2.87 \times 10^2\ m^2\ s^{-1}\ deg^{-1}$ is the (dry) gas constant, we readily find that

$$d(\ell n\ p) = - \frac{g}{R\bar{T}}\, dz\ .$$

Therefore

$$\frac{1000}{p} = e^{\frac{g}{R\bar{T}}(z-z_o)} \tag{6A}$$

where $\bar{T}$ is the logarithmically averaged value of T over the interval $z-z_o$ and z_o is the height at the 1000 mb level. Thus

$$\left(\frac{1000}{p}\right)^{-.286} \simeq 1 - 0.286 \frac{g}{RT}(z-z_o) + \frac{1}{2}\left[0.286 \frac{g}{R\bar{T}}(z-z_o)\right]^2 \ldots . \equiv f(z)$$

since $0.286 \frac{g}{RT}(z-z_o)$ is fairly small (i.e., < 0.29) for heights less than about 9 km. The next term in the expansion would contribute less than 0.4 of one percent at a height of 7.5 km — about the maximum height at the soundings reported by Thompson et al.

Finally, assuming an exponential density distribution of scale height H, equation (5A) gives

$$\rho_o e^{-z/H} = \frac{p}{R\bar{T}}$$

so

$$\frac{\partial p}{\partial z} = -\rho_o e^{-z/H} g\, dz = -\frac{RT}{H} \rho_o e^{-z/H}$$

or

$$H = \frac{R\bar{T}}{g} \tag{7A}$$

is the scale height for the height interval $z-z_o$. Therefore, in terms of N, H(T) and height z

$$\phi = e^{0.714z/H}[N\, f(z) + (77.6)(0.286)(p/T)z/H].$$

However from (5A) $P/T = \rho_o R\, e^{-z/H} \simeq 3.23\, e^{-z/H}$ for the Thompson et al. soundings at Denver assuming the 1000 mb density $\rho_o \simeq 1.13\times10^{3}$ gr m^{-3} and p is in millibars = 1000 dynes cm^{-2} = 10^{7} dynes m^{-2},

$$\phi = e^{0.714z/H}[N\, f(z) + 71.95(z/H)e^{-z/H}] \tag{8A}$$

$$\frac{\partial \phi}{\partial z} = H^{-1}e^{0.714z/H}[f(z)H\, \frac{\partial N}{\partial z} + 71.95(1-z/H)e^{-z/H} - 0.286N(1-6z/H)] + 0.714H^{-1}\phi \tag{9A}$$

To develop an expression for $C_\phi^{\,2}$ in terms of $C_n^{\,2}$, note that the perturbation ϕ' is related to N' as

$$\phi' \equiv d\phi = \frac{\partial \phi}{\partial N}\, dN$$

so from eq. (2A)

$$\phi' = N' e^{0.714z/H}\, f(z).$$

Therefore

$$C_\phi^{\,2} = e^{1.428z/H}\, f^2(z)\, C_n^{\,2}. \tag{10A}$$

REFERENCES

Fairall, C. W., R. Markson and J. Sedlacek (1977) Altitude dependence of C_T^2 over the ocean, Naval Post Graduate School Report NPS-61Fr 77101, 42 pp.

Gossard, E. E. (1953) The effect of wind on nighttime radiational cooling, Trans. Amer. Geophys. Union 34, 841-848.

Gossard, E. E. (1978) The height distribution of refractive index structure parameter in an atmosphere being modified by spatial transition at its lower boundary, Radio Science 13, 489-500.

Gossard, E. E., R. B. Chadwick, K. P. Moran, R. G. Strauch, G. E. Morrison, and W. C. Campbell (1978) Observation of winds in the clear air using an FM-CW Doppler radar, Radio Science 13, 285-289.

Hufnagel, R. E. (1974) Variations of atmospheric turbulence, Proceedings Topical Meeting on Optical Propagation through Turbulence, Optical Society of America.

Lenshow, D. H. (1974) Model of the height variation of the turbulence kinetic energy budget in the unstable planetary boundary layer, J. Atmos. Sci., 31, 465-474.

Metcalf, J. (1975), Microstructure of radar echo layers in the clear atmosphere, J. Atmos. Sci., 32, 362-370.

Ochs, G. R., and R. S. Lawrence (1972), Temperature and C_n^2 profiles measured over land and ocean to 3 km above the surface, NOAA TR ERL 251-WPL 22, 39 pp.

Thompson, M. C., F. E. Marler and K. C. Allen (1977), Measurements of refractive index parameters for calculating limits of SAR image resolution, Office of Telecommunications TM 77-233, 103 pp.

Van Zandt, T. E., J. L. Green, K. S. Gage and W. L. Clark (1978) Vertical profiles of refractivity turbulence structure constant: Comparison of observations by the Sunset radar with a new theoretical model, Radio Sci., 13, 819-829.

Wyngaard, J. C., Y. Izumi and S. A. Collins (1971), Behavior of refractive-index structure parameter near the ground, J. Opt. Soc. of Amer., 61, 1646-1650.

GPO: 1979--677-143/372